First published: 19 May 2020

Citation: J. Mater. Chem. C, 2020,8, 8290-8304

Specific features of the electronic and crystal structure of Cu_xZrSe_2 ($0 < x \leq 0.3$)

A. S. Shkvarin, A. I. Merentsov, Yu. M. Yarmoshenko, M. S. Postnikov, E. G. Shkvarina, E. V. Mostovshchikova, A. A. Titov, I. Pis, F. Bondino, S. A. Uporov, S. Yu. Melchakov and A. N. Titov, *J. Mater. Chem. C*, 2020, **8**, 8290 **DOI:** 10.1039/D0TC01884H

Specific features of the electronic and crystal structure of Cu_xZrSe_2 ($0 < x \leq 0.3$)

A. S. Shkvarin,[a] A. I. Merentsov, [a] Yu. M. Yarmoshenko, [a] M. S. Postnikov, [a] E. G. Shkvarina, [a] E. V. Mostovshchikova, [a] A. A. Titov, [a] I. Pis, [b,c] F. Bondino, [c] S. A. Uporov, [d] S. Yu. Melchakov [d] and A. N. Titov [a]

[a] *M.N. Miheev Institute of Metal Physics of Ural Branch of Russian Academy of Sciences, 620108 Yekaterinburg, Russia*

[b] *Elettra-Sincrotrone Trieste S.C.p.A, S.S. 14 – km 163.5, 34149 Basovizza,Trieste, Italy*

[c] *IOM-CNR, Laboratorio TASC, S.S. 14 – km 163.5, 34149 Basovizza, Trieste, Italy*

[d] *Institute of Metallurgy of Ural Branch of Russian Academy of Sciences, 620016, Yekaterinburg, Russia*

Abstract

Crystal and electronic structure, optical absorption and transmission spectra, temperature dependences of conductivity and magnetic susceptibility were studied for copper intercalated ZrSe2 in the copper concentration range of $0 \leq x \leq 0.3$. The electronic structure of CuxZrSe2 single crystals was studied at room temperature using X-ray Absorption Near Edge Structure spectroscopy (XANES), resonant photoelectron spectroscopy (ResPES) and optical absorption. The partial and total densities of states were calculated to determine the atomic contributions to the valence band. The competition between the occupation of octahedral and tetrahedral sites in the van der Waals gap by copper was found. The contribution of both positions to the formation of the chemical bond between copper and the ZrSe2 lattice with the domination of the Cu–Se interaction was determined. It was found that the intercalation of copper in the concentration range of x = 0–0.2 resulted in the formation of the localized impurity states in the Se 4p/Zr 4d band gap but not in the charge transfer to the conduction band. As the copper concentration increased above x = 0.2, the semiconductor-to-metal transition occurred due to the reaching of the conduction band by the Fermi level. The Se 4p/Zr 4d band gap was found to be a direct one in the whole studied concentration range. Some inconsistencies in the conductivity and spectral data along with the DOS calculation results were explained by the Frenkel defects in the ZrSe2 lattice.

Introduction

MCh_2 transition metal dichalcogenides, in which the metal and chalcogen atoms can be widely varied (M = Ti, V, Zr, Nb, Mo, Hf, W, Pt and Ch = S, Se, Te), have been studied over the past few decades.[1–6] These materials with a quasi-two-dimensional crystal structure exhibit some attractive physical properties. The MCh_2 dichalcogenides demonstrate such quantum effects as the charge density wave (CDW) state and superconductivity.[7–12] These materials are already used as cathode materials for lithium batteries,[13–20] photodetectors,[21–23] transistors with high electron mobility,[24] and

electronic devices.[25,26] The layered structure of MCh_2 allows the intercalation of atoms and molecules to modify the physical properties of the obtained material in a wide range. Limited interlayer space allows one to create nanosized inclusions[27] and one-dimensional chains of ordered intercalated atoms.[28–33] Intercalation compounds based on MCh_2 demonstrate important applied properties: superconductivity,[34–37] magnetism,[38–40] and thermoelectricity;[41,42] they can be used as solar cells,[43,44] electronic devices,[41,45] and battery systems.[13,46]

Zirconium diselenide $ZrSe_2$ is a structural analogue of titanium diselenide $TiSe_2$. In its turn, scientific interest to $TiSe_2$ is due to the CDW transition.[47] It has been reliably established that this state in $TiSe_2$ is associated with the so-called Keldysh– Kopaev mechanism of the transition to the excitonic insulator state.[48] There are convincing cases for the involvement of the phonon subsystem in the formation of this state.[49] A new interest in the study of $TiSe_2$ arose with the discovery of the superconducting transition in this material caused by a small external disturbance suppressing the excitonic insulator state. This transition was observed at high external pressure[50] or intercalation of a small amount of copper ions.[34] It is important to note that TiS_2, which is the closest structural analogue of $TiSe_2$, does not show any phenomenon like this one.

The substitution of Ti by heavier Zr in the host lattice MSe_2 leads to the enhancement of the polarization and therefore can lead to the increase of the quantum effects. In this work, we synthesized $ZrSe_2$ intercalated with copper and studied the crystal and electronic structure of these materials as well as their physical properties – conductivity and magnetic susceptibility in a wide temperature range, and optical absorption in the near infrared range at room temperature.

The crystal structure of $ZrSe_2$ is composed of a sequence of Se–Zr–Se layers (the so-called ‘‘sandwich’’) with strong covalent bonding inside the layers and a relatively weak bonding of the van der Waals type between the layers (Fig. 1). The experimental data on the crystal structure, calculation of the electronic structure of the initial $ZrSe_2$, and its electrical properties were first presented in ref. 51 and 52. In nonstoichiometric $ZrSe_2$ intercalated with copper the superconducting transition occurs,[53] which draws an additional interest to the Cu–$ZrSe_2$ system. The electronic structure of these materials was previously studied in ref. 54 and 55.

It has been shown for Cu–TiS_2[56,57] that the instability of the layered modification is associated with the occupation by intercalated atoms of the sites in the interlayer space, which are tetrahedrally coordinated by the sulfur atoms. Therefore, the study of the stability of the layered modification of the intercalation materials requires information about the distribution of intercalated atoms between the octahedral and tetrahedral sites in the interlayer space. This information can be obtained from the full-profile refinement of the X-ray diffraction patterns. The ordering of the intercalated atoms with a decrease in the crystallographic symmetry, observed in ref. 30–33 and 58, significantly complicates this task. To avoid these difficulties, we have chosen the concentration range of $0 < x \leq 0.3$ for Cu_xZrSe_2, in which copper atoms are not ordered. This concentration range is similar to that ($0 < x < 0.12$) for the Cu_xTiSe_2 system,[34] in which the CDW state and superconductivity are observed.

The crystal structure of the obtained materials was studied by powder X-ray diffraction using the full-profile refinement procedure, the electrical conductivity was measured for polycrystalline samples in the temperature range of 10–300 K, and the magnetic susceptibility was measured for

polycrystalline samples in the temperature range of 3–300 K. The electronic structure of Cu_xZrSe_2 single crystals was studied at room temperature using Cu $L_{3,2}$ X-ray absorption near edge structure spectroscopy (XANES), resonant photoelectron spectroscopy (ResPES) and optical absorption spectroscopy.

Experimental

Cu_xZrSe_2 polycrystals were synthesized using a room-temperature solid-state reaction technique from the preliminarily prepared $ZrSe_2$ powder and finely dispersed copper. The synthesis technique of $ZrSe_2$ is described in more detail in ref. 59. The intercalation procedure is described in detail in ref. 56. The single crystals of Cu_xZrSe_2 with x = 0.1, 0.2, 0.3 were grown in quartz ampoules using a gas-transport reaction technique with I_2 as a gas-carrier at a temperature of 850 °C, as reported in ref. 60. The chemical composition of the crystals was determined using X-ray energy dispersive analysis (EDA) on an ‘‘Inspect F’’ scanning electron microscope.

The crystal structure of the $ZrSe_2$ and Cu_xZrSe_2 powders was determined using X-ray powder diffraction (XRD) on a Shimadzu XRD 7000 Maxima diffractometer (Cu Ka_1 radiation, graphite monochromator, 2Y = 5–901). The crystal structure refinement was performed using the GSAS (General Structure Analysis System) software package.[61] Background was approximated by the Chebyshev polynomial with 8 coefficients. For all samples, the following model of the crystal structure was used: P-3m1 space group (164),[62] atomic positions Zr(1a) (0 0 0), Se(2d) (1/3 2/3 z), Cu1(1b) (0 0 1/2) (octahedral sites), Cu2(2d) (1/3 2/3 z) (tetrahedral sites)[62] (see e.g. Fig. 1). The atomic coordinates of the selenium and copper atoms in the tetrahedral sites along with the occupation of the octahedral and tetrahedral sites by the copper atoms were refined. Site occupancy fractions for Cu1(1b) and Cu2(2d) were constrained by total copper concentration taking into account the multiplicity of these sites. A pseudo-Voigt function with a Finger–Cox–Jephcoat peak asymmetry correction (peak profile type No. 3) was used for the profile fitting. Anisotropic displacement parameters were used for the Zr and Se atoms in the refinement.

The XANES and ResPES spectra were obtained at the CNR BACH beamline[63] of the Elettra synchrotron facility (Trieste, Italy). Linearly polarized X-rays with a polarization vector 60° off the surface plane were used. All the samples were cleaved in situ in a vacuum chamber at a pressure lower than 1×10^{-9} Torr. The purity of the surface was confirmed by the absence of oxygen and carbon peaks in the survey spectra. A VG-Scienta R3000 hemispherical analyzer set at 60° off the incoming X-ray beam was used for photoemission measurements. Valence band spectra were measured in a normal emission geometry with a total energy resolution of 0.15 eV. Photoemission binding energies were calibrated using the Fermi edge measured on a gold reference. Cu $L_{2.3}$ XANES were acquired in total electron yield mode with an energy resolution of 0.2 eV and calibrated using the Au VB spectrum on the Fermi edge with corresponding excitation energy.

First principles calculations were performed to obtain a theoretical description of the density of states of the studied materials near the Fermi level. Total density of state (TDOS) and partial density of states (PDOS) calculations were performed using the full-potential linearized augmented plane wave (FP-LAPW) approach and the generalized gradient approximation in the Perdew–Burke–Ernzerhof variant (GGA-PBE)[64] exchange–correlation functional in the ELK software package.[65] Integration over the Brillouin zone was carried out using an 8×8 ×8 grid of special k points, and the

total number of k-points was 176. The selfconsistent calculation was finished when the total energy change became less than 0.0001 eV. Experimentally determined parameters of the crystal structure were used in these calculations. For calculations the ‘‘Uran’’ supercomputer of IMM UB RAS was used.

Electrical resistivity was measured in the temperature range of 10–300 K by means of a standard direct-current two-probe technique using a closed-cycle helium cryostat with a SRDK-205D (Sumitomo, Tokyo, Japan) cryo cooler on polycrystalline samples. Low cooling and heating rates (1 K min^{-1}) were used to make measurements as balanced as possible.

Magnetic susceptibility w was measured in the temperature range of 3–300 K and a magnetic field of 1 kOe on a vibrating sample magnetometer (VSM) system CFS-9T-CVTI (Cryogenic Ltd, UK). Polycrystalline samples were placed into a weakly magnetic gelatin capsule. The signal from the capsule was subtracted from the obtained temperature dependence of the magnetic susceptibility during the data processing.

The optical studies were carried out in the near-IR range in the photon energy interval of $0.15 < \hbar\omega < 1.1$ eV at 295 K using a prism spectrometer. The absorption spectra $\alpha(\hbar\omega)$ were calculated from the experimentally obtained transmission spectra of $t(\hbar\omega)$ using the following formula:

$$\alpha(\hbar\omega) = [1/d]\ln[(1 - R(\hbar\omega))^2/t(\hbar\omega)] \quad (1)$$

where d is the thickness of the sample, $t(\hbar\omega) = I/I_0$ is the sample transmittance (I is the intensity of the light passed through the sample, I_0 is the intensity of the light in the incident beam), $R(\hbar\omega)$ is the reflection measured previously from the same sample. The samples were single crystals with a thickness d of about 20–40 mm. The crystals for the optical measurements were cleaved directly before measuring. The measurement time for one sample was about 20 minutes. The intensity of the light transmitted through the sample recorded at the end of the measurement coincided with that recorded at the beginning (within measurement accuracy). Therefore, we suppose that the contamination of the sample surface during measurement, if any, can be neglected.

Experimental results

Crystal structure

The crystal structure of Cu_xZrSe_2 is described in the P-3m1 space group in the whole studied Cu concentration range ($0 \le x \le 0.3$).

This indicates the stability of the layered form of the material in this Cu concentration range. The superstructure lines are not observed; this indicates that there is no ordering of the intercalant, as it was expected, when this concentration range was chosen. The full-profile refinement procedure was used to obtain and analyze the information about the copper distribution between octahedral and tetrahedral sites in the interlayer space. The refinement results are listed in Table 1.

The dependence of the fraction (in %) of copper atoms that occupy tetrahedral and octahedral sites on the total copper concentration is shown in Fig. 2a. As it can be seen from Fig. 2a and Table 1, at a low ($x \le 0.1$) copper concentration, almost all copper atoms occupy tetrahedral sites of the

interlayer space and the copper atom is displaced toward the base of the tetrahedron (Fig. 1 and 2b, right panel). This position of the copper atom is energetically favorable due to a large difference in the components of the Young's modulus e in the xy direction (basal plane) and z direction for all the compounds of the CdI_2 type. For $ZrSe_2$, $e_x = e_y = 90.041$ GPa, which substantially exceeds $e_z = 5.8398$ GPa.[66] This suggests a weaker elastic distortion of the lattice at the occupation by copper of the octahedral sites than that at the occupation of the tetrahedral ones. Hibma first wrote about this;[67] in that work the phase stability in intercalation compounds was associated with the elastic distortions at the occupation of the tetra- and octahedral sites. The same approach made possible a quantitative description of the diffusion of silver in TiS_2.[68] The interaction of the 3d4s electrons of the intercalated ion in the octahedral sites with the electrons of the transition metal atom in the second coordination sphere of the host lattice was confirmed experimentally[69] and by the theoretical calculations.[70] In the case of the occupation of the tetrahedral sites the chalcogen atoms are in the nearest environment of the intercalated atom, and no orbitals of the intercalant are directed to the host lattice transition metal. In this case the only Cu 3d, 4s/Se 4p hybridization is possible. In the copper concentration range of $0 \le x \le 0.2$ the increase in x leads to the partial transfer of the copper atoms from the tetrahedral sites to the octahedral ones, in which Cu 3d, 4s/Se 4p/Zr 4d hybridization is possible.

At $x = 0.2$ the copper atoms in the tetrahedral sites are shifted to the middle of the interlayer space, and the Z coordinate of copper atoms in the tetrahedral sites is equal to that of copper atoms in octahedral sites ($Z_{Cu} = 0.5$); this is accompanied by the contraction of the van der Waals gap (Fig. 2c) and the increase in the thickness of the Se–Zr–Se sandwich (Fig. 2d). As a result, As a result, the Cu0.2ZrSe2 composition corresponds to the minimum on the concentration dependence of the van der Waals gap width (see Fig. 2c) and to the largest filling of the octahedral sites with copper atoms (37% of the total copper content). At x Z 0.25 the copper atoms occupy the centres of the tetrahedron's inscribed sphere. This position is most favourable in the case of the absence of other interactions than elastic ones. Therefore, a further increase in the copper content leads to the transfer of copper from the octa- to tetrahedral sites, which provides the prevalence of Cu 3d, 4s/Se 3p hybridization (see Fig. 2a). The filling of the tetrahedral sites with copper atoms increases and the interlayer space expands.

Electronic structure

X-ray photoemission core level spectra for Cu_xZrSe_2 ($x = 0–0.3$) were published earlier[55] and showed the monotonic increase in the Zr 3p and Se 3d binding energies. This behavior was explained by the gradual shift of the Fermi level with increase in copper concentration. The width of the core level peaks didn't depend on the copper concentration, which indicated the weak effect of the environment geometry on the core level binding energies.

XANES

The Cu $L_{2,3}$ XANES for Cu_xZrSe_2 are shown in Fig. 3. These spectra differ from those for Cu_xTiSe_2, where copper atoms act at low concentration ($x < 0.2$) like free ions.[71,72] In contrast, in Cu_xZrSe_2 copper atoms interact even at low concentration with the arrangement, and the type of chemical bond changes with the increase in the copper concentration. The spectra for $Cu_{0.1}ZrSe_2$ and

$Cu_{0.3}ZrSe_2$ are almost identical in shape and energy position of the peaks and differ from the spectrum for $Cu_{0.2}ZrSe_2$, for which the main band C is broadened, its intensity is lower and its energy position is shifted toward high photon energies by 0.5 eV. This broadening and energy shift can be explained by the appearance of an additional contribution to the absorption spectrum. The structural data suggest (Table 1) that in $Cu_{0.2}ZrSe_2$ the occupation of octahedral sites by the copper atoms becomes more pronounced in addition to the occupation of tetrahedral sites. Since the local arrangement of the Cu atoms in these crystallographic positions differs significantly (4 chalcogen atoms for tetrahedral sites and 6 chalcogen atoms for octahedral ones), two different contributions to the absorption spectrum should be observed. Bearing in mind that only tetrahedral sites are occupied in $Cu_{0.3}ZrSe_2$ and both tetra- and octahedral sites are occupied in $Cu_{0.2}ZrSe_2$ (with a ratio of 1:2), we can obtain the contribution of the octahedral sites (Fig. 3, lower panel, black line). To do this, we need to subtract the intensity of the $Cu_{0.3}ZrSe_2$ spectrum multiplied by $2/(1 + 2) = 0.66$ from the intensity of the $Cu_{0.2}ZrSe_2$ spectrum. As one can see from the Fig. 3, lower panel, the so-obtained difference spectrum and Cu $L_{2,3}$ XANES for $Cu_{0.33}TiSe_2$, in which copper atoms occupy only octahedral sites, are similar in shape and energy position. So, we can conclude that the shape of the Cu $L_{2,3}$ XANES depends on the crystallographic position of copper atoms: it is similar to that for $Cu_{0.3}ZrSe_2$ in the case of copper atoms occupying the tetrahedral sites and to that for $Cu_{0.33}TiSe_2$ in the case of copper atoms occupying octahedral sites.

ResPES

Resonant photoelectron spectroscopy provides element-specific information on the energy localization of the electronic states in a valence band. The choice of the incident photon energy slightly larger than the binding energy of the selected core level upon excitation of the np electrons (n = 2; 3; 4) to an unfilled nd state leads to the increase in the intensity of the photoemission of d electrons from nd metals and their compounds, resulting in a resonant electron emission.[73–76] This effect is interpreted as resulting from a coherent process in which an np electron in the initial state is excited to an empty nd level to form an intermediate bound state (np, nd). The energy of the resonance maximum corresponds to crossover emergence (i.e., the transition from the RRAS (resonant Raman-Auger spectra) to the normal Auger spectra).[77]

Since the photoionization cross-section of the Zr 4d level ($s_{Zr} = 0.0493$ mb) is small in comparison with that of Se 4p*2 ($s_{Se} = 0.986$ mb) at a Zr 3p–4d resonance excitation energy (320–340 eV),[78] the intensity of the resonance bands is very low. Therefore, it is difficult to identify the resonance band even analyzing the difference spectra.[79] The valence band spectra almost do not change with a change in the excitation energy for all samples (Fig. 4).

A band with a binding energy of about 3.8 eV is observed in the valence band spectra (highlighted by gray ellipse) obtained in the Cu 3p–3d resonant excitation mode for $Cu_{0.2}ZrSe_2$ (Fig. 4). This band is also observed for $Cu_{0.3}ZrSe_2$, but its intensity is substantially weaker. Another band is observed in a wide binding energy range (5–14 eV), the intensity of which gradually decreases starting from $E_{exc} = 75$ eV. The appearance of a resonant Cu 3p–3d band with $E_b = 3.8$ eV indicates the presence of the Cu 3d states in the valence band. The decrease in the intensity of the resonant band mentioned above is associated with a substantially different scale of the change in the values of the photoionization cross-section for Cu 3d, Zr 4d and Se 4p states (see Fig. 5, the values were taken according to ref. 78). These states give the most significant contribution to the valence band of Cu_xZrSe_2.

The most significant change in the photoionization crosssection in the excitation energy range of 70–85 eV is observed for Zr 4d states (≈30%), while for Cu 3d and Se 4p this change is less pronounced (≈10%). Since a noticeable change in the ResPES spectra is observed only for $Cu_{0.2}ZrSe_2$, the Zr states in this material should differ from those in other Cu_xZrSe_2 (x = 0.1, 0.3) compounds. This difference is caused by the significant occupation of the octahedral sites by the copper atoms and, consequently, by the formation of the Zr–Cu chemical bonds in $Cu_{0.2}ZrSe_2$.

DOS calculation

To determine the energy position of atomic states in the valence band, the partial and total densities of states were calculated. The calculation was performed for two compositions – $Cu_{0.125}ZrSe_2$ and $Cu_{0.25}ZrSe_2$. To simulate the intercalation of cooper, a supercell, which contains eight $ZrSe_2$ formula units, was used. In the case of $Cu_{0.125}ZrSe_2$ one copper atom was placed into the position in the interlayer space, while in the case of $Cu_{0.25}ZrSe_2$ two copper atoms were placed into the positions in the interlayer space at the maximal distance from each other. The space group of the supercell P-3m1 (164) was taken the same as for the host lattice. The lattice parameters and ‘‘z’’ coordinate of the selenium and cooper atoms were obtained from the Rietveld refinement of the diffraction patterns for the corresponding polycrystalline samples (Table 1).

Cu s, p, d partial DOS for $Cu_{0.125}ZrSe_2$ and $Cu_{0.25}ZrSe_2$ are shown in Fig. 6a–c. The most pronounced changes at the Fermi level are observed for the Cu p states. The Se s, p partial DOS (Fig. 6d and e) increases proportionally with copper concentration, but the increase is nearly the same both for s and d states. Finally, the Zr s, p, d partial DOS (Fig. 6f–h) does not show pronounced changes either for different copper concentrations or for different states.

Magnetic susceptibility

The temperature dependencec of the magnetic susceptibility for Cu_xZrSe_2 ($0.05 \le x \le 0.25$) is of the Pauli type (Fig. 7, left panel). This indicates the conservation of the Cu d^{10} configuration and allows the density of electronic states at the Fermi level $\rho(E_F) = \chi/\mu_B^2$ to be calculated (Fig. 7, right panel). Therefore, a decrease in DOS upon copper intercalation can be interpreted as a corresponding shift of the Fermi level, which is located in the energy gap, from the Se 4p valence band towards the Zr 4d conduction band.

As it has been shown experimentally,[55] the increase in the Zr 3p, Zr 3d and Se 3d binding energies (E_b) in Cu_xZrSe_2 in the concentration range of x = 0–0.2 is caused by the 1 eV shift of the Fermi level. At x > 0.2 the slope of the $E_b(x)$ concentration dependence sharply decreased, which was explained by the increase in the density of states at the Fermi level, because the Fermi level reached the bottom of the conduction band. This makes possible the estimation of the Se 4p/Zr 4d energy gap width in the initial zirconium diselenide as approximately 1 eV, which is consistent with the available literature data.[51] On the other hand, this indicates that at x = 0 the Fermi level coincides with or is very close to the top of the valence band. The effective mass of the holes in transition metal dichalcogenides is much higher than that of the electrons.[80] Doping by electrons at the copper intercalation shifts the Fermi level to the region of the Se 4p/Zr 4d energy gap. This is manifested in the observed sharp decrease in the magnetic susceptibility. In the region of the gap, the density of states does not drop to zero, probably due to the presence of impurity levels.

This conclusion is consistent with smooth rather than sharp concentration dependence of E_F, which was observed in ref. 55 for the copper concentration range of $0 < x < 0.2$ and was associated with the formation of the Cu 3d, 4s/Zr 4d or Cu 3d, 4s/Se 4p covalent centers. The absence of the Zr 4d contribution to the ResPES for $Cu_{0.1}ZrSe_2$ and $Cu_{0.3}ZrSe_2$, in which the main part of the copper atoms is located in tetrahedral sites, allows us to identify these centers as Cu 3d, 4s/Se 4p ones.

Electrical properties

The temperature and concentration dependences of the electrical resistivity for Cu_xZrSe_2 are shown in Fig. 8. The sharp decrease in the resistivity value even at small copper concentration (Fig. 8, right panel) indicates that the intercalation leads to the electron transfer from the copper atoms to the lattice. Semiconducting behavior of the temperature dependence of the resistivity (Fig. 8, left panel), the decrease in the density of states at the Fermi level (Fig. 7, right panel) and the smooth dependence of E_F on the copper concentration in the copper concentration range of $0 < x < 0.2$[55] indicate that the electron transfer occurs not to the conduction band but to the impurity level located in the energy gap between the valence and conduction bands. The temperature dependence of the normalized resistivity for Cu_xZrSe_2 (Fig. 8, left panel) gradually changes from the semiconducting behavior at $x < 0.2$, which indicates the localized character of electrons introduced at the intercalation process, to the metallic one at $x > 0.2$. This is in good agreement with the conclusion about the covalent nature of the chemical bond between the copper ions and the host lattice based on the analysis of the crystal and electronic structure and magnetic susceptibility. The obtained temperature dependence of the resistivity for $ZrSe_2$ is in qualitative agreement with the previously published data (e.g. ref. 81), in which it demonstrates the semiconducting behavior with two activation energies: $E_{a1} = 0.0587$ eV in the temperature range of 303–393 K and $E_{a2} = 0.187$ eV in the temperature range of 393–443 K. Plotting $\ln(\rho/\rho_{300})$ vs. 1/T (Fig. 9, left panel), we observe similar temperature dependences of the resistivity (however, in the other temperature regions, which is due to the lower values of the activation energies), which could be also described using two values of the activation energy. This suggests the presence of two types of defects that generate impurity levels with different binding energies in the energy gap. Excess metal in the interlayer space is the most common and stable defect in transition metal dichalcogenides. The second type of defect can be associated with vacancies in the zirconium or selenium sublattice. Since the conduction band is empty in undoped $ZrSe_2$, a lower activation energy value E_{a1} should be associated with an acceptor level close to the top of the valence band. This level can be formed by the Zr vacancies, probably due to the presence of Frenkel defects. The level with higher activation energy E_{a2} should be associated with the donor level formed by the interlayer zirconium. The conservation of the semiconducting behavior at copper concentrations $x < 0.2$ indicates that the interlayer copper atoms act like interlayer zirconium atoms and generate donor levels. The explanation suggested is in a good agreement with the dependence of the activation energies on the copper concentration in Cu_xZrSe_2 (Fig. 9, right panel). Actually, the energy of the lower level is almost independent of x. This indicates the absence of the interaction of the intercalated Cu atoms with Zr vacancies. It looks quite natural, because the nearest copper environment consists of the selenium atoms.

The decrease in the activation energy E_{a2} associated with the interlayer metal atoms can be explained by the lower binding energy of the Cu^{+}-derived level compared to the Zr^{4+}-derived one. Moreover, the concentration of copper is much higher than the excess of zirconium. This follows from the Zr 3p core level spectra, where we do not observe the contribution from excess Zr,[55] while in ref. 54 this contribution is substantial. Inevitably, this should lead to an increase in the width of the impurity level, which even can overlap with the conduction band as the copper concentration increases. Probably, it is something that occurs at $x > 0.2$ – the band formed by the intercalated copper overlaps with the $ZrSe_2$ conduction band and the Fermi level goes above the energy gap, as it follows from the calculations of the electronic structure (Fig. 6). A further increase in the copper concentration leads to a further broadening of the impurity band and the charge transfer to the $ZrSe_2$ conduction band. It is obvious that the impurity states formed by the copper atoms, which occupy the tetrahedralsites, lie directly below the Fermi level. In our opinion, the proposed mechanism explains the observed increase in the occupation of tetrahedral sites at $x > 0.2$.

Optical properties

Fig. 10 shows the transmission and absorption spectra (t(E) and α(E)) for the ZrSe2 and CuxZrSe2 (x = 0.05, 0.15) single crystals.

The transmission spectra for the studied single crystals are different for the undoped zirconium diselenide and for doped ones. It is seen that for $ZrSe_2$, the transmission increases in the low-energy part of the spectrum, reaches the maximum at E = 0.8 eV and then decreases. For the Cu-intercalated crystals, the transmission decreases with the energy slowly below 0.6 eV and more quickly at higher energy. A set of peaks in the t(E) spectra for $Cu_{0.05}ZrSe_2$ and $Cu_{0.15}ZrSe_2$ crystals in the low energy region can be associated with the vibrations of carbon or hydroxyl associated molecules adsorbed on the crystal surface. The question about the nature of the IR bands in the energy range of 0.2–0.6 eV is out of the scope of the present work. Additional investigations will be carried out. However, one can assume that the H_2O and CO molecules absorbed on the crystal surface may contribute to the optical spectra, because all the optical spectra were obtained in air. The presence of these molecules is usual in this case.[82]

The absorption coefficient a of the initial $ZrSe_2$ is rather high. The increase of the absorption in the high-energy region of the spectrum is associated with the beginning of the fundamental absorption. In the low-energy region of the spectrum the absorption increases with the decrease of the energy, and this increase begins at about 0.8 eV. This increase is not associated with the tails of the phonon bands. As it is shown in ref. 83, the highest energy of the phonons in $ZrSe_2$ is calculated as 255.2 cm^{-1} (~31.6 meV). In the ‘‘transparency window’’ (the region of the spectrum between the region of the interaction of the light with the optical phonons and the fundamental absorption range) the minimal value of the absorption coefficient is about 800 cm^{-1}. The high absorption in the ‘‘transparency window’’ masks the fundamental absorption edge. Such behavior of the α(E) curve indicates the presence of the delocalized charge carriers and does not agree with the activation character of the ρ(T) dependence. This can be explained supposing the nonuniform charge state: there are some regions with a metallic character of the resistivity, which are separated from each other. These regions can be agglomerations of the defects in the form of the interlayer zirconium

atoms. It is well known that this type of defect is typical for layered transition metal dichalcogenides.

The intercalation of copper into $ZrSe_2$ results in significant decrease in the absorption coefficient. This is probably due to the compensation of the valence band holes by the electrons introduced with copper atoms. The increase of the absorption coefficient with decreasing energy is not observed for Cu_xZrSe_2 as it is for $ZrSe_2$. The shape of the $\alpha(E)$ curve for both $Cu_{0.05}ZrSe_2$ and $Cu_{0.15}ZrSe_2$ crystals is one which is typical for semiconductors. The value of the absorption coefficient near the fundamental absorption edge is about 100 cm^{-1} for

$Cu_{0.05}ZrSe_2$ and 150 cm^{-1} for $Cu_{0.15}ZrSe_2$. As it is shown above, the resistivity has semiconductor character: r increases with the temperature decrease in the whole measured temperature range ($10 < T < 300$ K) in initial $ZrSe_2$ and $Cu_{0.05}ZrSe_2$. In $Cu_{0.15}ZrSe_2$ the resistivity decreases with temperature down to $T \sim 150$ K and increases with further cooling. The difference between optical and transport data can be explained by assuming that copper intercalation affects the defect structure of the material. For example, the holes generated by zirconium vacancies can be compensated by the electrons introduced with intercalated copper.

Depending on the relative position of the extrema of the valence and conduction bands the interband transitions are divided into direct and indirect ones. In the case of the direct transitions the energy dependence of the absorption coefficient in the range of the optical absorption edge is described by the relation

$$\alpha = [A(\hbar\omega - E_g^d)^n]/\hbar\omega, \qquad (2)$$

where α is the absorption coefficient, $\hbar\omega$ is the photon energy, E^d_g is the direct optical band gap, A is a constant and exponent 'n' depends on the type of transition and may have values 1/2 (or 3/2 if the forbidden direct transitions occur).[84]

If the indirect interband transitions occur in the crystals, the determination of the indirect band gap (E^i_g) must take into account the absorption and emission phonons which allow the indirect transition. Therefore, the absorption coefficient a for a single-phonon process can be expressed as

$$\alpha = [B(\hbar\omega - E_g^i \pm E_p)^m]/\hbar\omega, \qquad (3)$$

where E^i_g is the indirect energy gap, E_p is the energy of the absorbed (+) or emitted (-) phonon, m = 2 for allowed indirect transitions and m = 3 for forbidden indirect transitions.[85]

Moustafa et al.[86] have reported both direct and indirect interband transitions for $ZrSe_2$, although they mentioned that all calculations were carried out using different methods.[87–90] In ref. 86 the values of direct and indirect energy gaps were estimated to be 1.2 eV and 1.6 value, correspondingly. To conclude the type of optical transition in the crystals under study we have plotted the experimental absorption spectra in coordinates $(\alpha\hbar\omega)^2$ vs. $\hbar\omega$, and $(\alpha\hbar\omega)^{1/2}$ vs. $\hbar\omega$ (Fig. 11).

Fig. 11 illustrates determination of the indirect (upper panel) and direct (lower panel) band gap values as an intersection of the straight line, which is the linear extrapolation of the experimental

curve, with the photon energy axis ($\alpha = 0$). It is seen, that the E^i_g values of 0.2–0.4 eV (depending on the concentration of the intercalated copper) are too small in comparison with those estimated theoretically[87–90] and with those reported in ref. 86. Moreover, it is impossible to get satisfactory fitting of the experimental data with the phonon energy E_p near 30 meV. The fitting gives much higher value of E_p. The value of the E^i_g increases with copper concentration, which is only possible in the case of the ZrSe2 lattice distortion, which is in fact not observed. All of the above indicates that the energy gap in CuxZrSe2 crystals is not indirect.

The direct energy gap values E^d_g were determined as the intersection of the linear extrapolation of the $(\alpha\hbar\omega)^2$ vs. $\hbar\omega$ curves with the E axis (a = 0) (Fig. 11, lower panel). The value of E^d_g for ZrSe2 is estimated as about 0.8 eV and is almost independent of the copper concentration in CuxZrSe2. It should be noted that the value of the gap for ZrSe2 is slightly underestimated, because there is strong absorption near the absorption edge, which is possibly contributed from the charge carriers. It is seen that for ZrSe2 the linear fit of the $(\alpha\hbar\omega)^2$ vs. $\hbar\omega$ experimental points is not so good as for Cu0.05ZrSe2 and Cu0.15ZrSe2. This can be associated with Urbach tailing of the absorption edge, which is typical for amorphous or disordered materials and obeys the empirical expression

$$\alpha = \alpha_0 \exp(\hbar\omega - E_0/E_U), \qquad (4)$$

where α_0 and E_0 are characteristic parameters of the material, and E_U is the Urbach energy.[58] As it is shown in ref. 85, an Urbach tail can coexist with the indirect or direct absorption edge. Therefore, the plots of the $\ln(\alpha)$ vs. $\hbar\omega$ near the absorption edge can be represented by an approximated straight line for energies just below the fundamental absorption edge. It is clearly seen on the inset in Fig. 11, lower panel, that the absorption spectrum for ZrSe2 plotted in ln(a) vs. $\hbar\omega$ coordinates is well described by the straight line. The exponential character of the absorption coefficient in the tail of the absorption edge points to the presence of some disorder in the $ZrSe_2$ crystal. This disorder is caused by the Zr vacancies mentioned above.

Discussion

The experimental data show a consistent picture: the intercalation of copper into $ZrSe_2$ leads to a transition from the activation resistivity in the copper concentration range of $0 < x < 0.2$ to the metallic resistivity at $x > 0.2$. However, the activation energy values, calculated from the temperature dependence of the resistivity, significantly differ from the band gap values, calculated both from the optical absorption spectra (the current study) and from the X-ray spectroscopy data.[55] While the band gap width in the $ZrSe_2$ is approximately 0.8–1.0 eV, the activation energy does not exceed 30 meV. The reason for this difference may be the presence of extra zirconium. This type of defect is typical for the transition metal dichalcogenides.[91] Since, according to ref. 92, the extra zirconium atoms occupy octahedral sites in the interlayer space, its local arrangement is close to that of zirconium within a sandwich.

However, the presence of the extra zirconium does not lead to metal conductivity. It means that extra zirconium does not transfer its valence electrons to the conduction band. Therefore, it can be expected that extra zirconium should create an impurity level in the $ZrSe_2$ band gap. The same

octahedral arrangement of this extra zirconium and zirconium in a regular lattice suggests that the impurity level should be located very close to the bottom of the conduction band. In this case the observed activation energy may be associated with this level, and its dependence on the copper content indicates the interaction between copper atoms in the interlayer space. This also may be a reason for the observed discrepancies with the optical data. The absorption optical spectra demonstrate the fundamental absorption, and contain information about the width of the intrinsic gap of $ZrSe_2$, whereas the temperature dependence of the resistivity is determined by the excitation of the electrons from the impurity level formed by the extra zirconium. The independence of the optical gap on the copper concentration is explained by the formation of impurity states in the band gap involving the states of intercalated copper atoms and indicates a relatively weak interaction between the copper ions and the host lattice.

The nonmonotonic copper concentration dependence of the occupation of the tetra- and octahedral sites by copper atoms in the studied concentration range indicates a significant change in the electronic structure caused by the intercalation. Information about the electronic structure allows us to understand the influence of the copper intercalation on the properties of the material. According to our previous data, $ZrSe_2$ is a semiconductor with a direct gap of nearly 1 eV,[55] while the data of the current article suggest the value of the direct gap of $E_g = 0.8$ eV. As it can be seen from ref. 55, the intercalation of copper leads to an increase in the Fermi energy. Moreover, the $E_F(x)$ dependence is almost linear up to $x = 0.2$. The shift of the E_F in this concentration range equals 1 eV, which coincides with the band gap width in $ZrSe_2$.[51] This suggests that the initial position of the E_F coincided with the top of the valence band. Therefore, a change in the slope of the $E_F(x)$ dependence for $x > 0.2$[55] can be associated with an increase in the density of states at the Fermi level when it reaches the bottom of the conduction band or with the formation of an impurity band overlapping with the conduction band. The second explanation seems to be preferable, because if the Fermi level were in the conduction band, it would result in a significant increase in the Pauli susceptibility and an appearance of a resonant Zr 4d peak in ResPES.

The occupation of the octahedral sites by copper in the concentration range of $0 < x < 0.2$, may be caused by the thermal activation of copper from the tetrahedral sites. This is confirmed by the almost linear increase in the occupation of the octahedral sites with increase in copper concentration (Fig. 2). In the octahedral sites copper atoms form mainly ionic bonds with the lattice, while in tetrahedral sites copper atoms form covalent bonds with selenium. At $x > 0.2$, the impurity band of the Cu states merges with the conduction band, so the Fermi level becomes in the conduction band. This is confirmed by the transition from the activation resistivity at $x < 0.2$ to the metallic one at $x > 0.2$, by an increase in the density of states at the Fermi level, and by the results of calculations of the electronic structure. At $x > 0.2$, the states of the copper atoms, which are tetrahedrally coordinated by selenium, are located below the Fermi level due to more favorable arrangement of the copper atom within the tetrahedron (see Fig. 1). This makes the occupation of the tetrahedral sites more energetically preferable since the electrons occupy these states instead of the electron transfer to the Fermi level in the conduction band. We suppose that it leads to an increase in the occupation of the tetrahedral sites with an increase in x at $x > 0.2$.

Therefore, the reason for the significant occupation of the tetrahedral sites is the width of the energy gap, which in $ZrSe_2$ is much higher than that for the intercalation compounds based on

$TiCh_2$, Ch = S, Se, Te. It can be concluded that the reason for the filling of only the octahedral sites in A_xTiCh_2 is the absence or small width of the energy gap between the Ch np-derived valence band and Ti 3d-derived conduction band. The spatial orientation of the low-energy Ti $3d_{zz}$ orbital, which is directed strictly to the intercalated atom and stabilizes the Ti–A covalent bond, is a key in this case. As soon as the width of the energy gap in Cu_xZrSe_2 becomes equal to that in $ZrSe_2$, the Cu–Se covalent bond as in binary[93,94] or complex[95,96] copper selenides becomes favorable.

It can be assumed that a similar mechanism determines the type of crystallographic position occupied by an intercalant A in transition metal dichalcogenides MCh_2 with 1T crystal modification. In the case of a wide band gap between the M nd conduction band and the Ch np valence band, electron transfer is more favorable into the A/Ch impurity state formed by the intercalated atoms and their tetrahedral arrangement. An alternative could be the octahedral coordination of the intercalated atoms, accompanied by an electron transfer to the M nd conduction band. This could lead to energy costs equal to the energy gap between the impurity states formed by the tetrahedrally coordinated intercalated atoms and the bottom of the conduction band. If the band gap is large enough, the energy gain due to the formation of an impurity state by tetrahedrally coordinated intercalated atoms may turn out to be large enough to make the tetrahedral coordination of the intercalated atoms energetically more favorable than the octahedral one. In the case of semimetallic compounds with a small overlap of Ch np- and M nd-derived bands (e.g. about 600 meV for $TiTe_2$[97,98]) or compounds with a narrow Ch np–M nd band gap (e.g. 150 20 meV for $TiSe_2$[99]), this energy gain is either completely absent or negligible compared to the thermal energy of the intercalated atoms, even at room temperature. In materials with a noticeable, but not wide yet, band gap (e.g. TiS_2, E_g = 0.5 eV,[100] $ZrSe_2$, E_g = 1.1 eV[51]), the energy gain at the occupation of the tetrahedral sites is small, but quite noticeable. This leads to a strong temperature (as for Cu_xTiS_2) or concentration (as for Cu_xZrSe_2) dependence of the prevalent occupation of the tetrahedral or octahedral sites. Since the band gap width in all the studied transition metal dichalcogenides decreases with the external pressure, it can be expected that the quantum states like CDW or superconductivity, which are typical for the materials with octahedrally coordinated intercalated atoms, can be observed in the materials with Ch np–M nd band gap of 0.5–1 eV at an applied external pressure. We expect that external pressure can be responsible for a change of the prevalent tetrahedral coordination of the intercalated atoms to an octahedral one.

In contrast to many other layered compounds, $ZrSe_2$ does not have stable polymorphs. Therefore, one can expect that the intercalation will lead to a change in the lattice parameters without change in the local arrangement of the Zr atom. The occupation of only the positions in the van der Waals gap by the intercalated atoms should lead to a break of the twodimensionality of the material. In this context, the intercalation affects the properties of the layered materials in a similar way to the pressure; the latter also leads to the rapprochement of the adjacent Ch–M–Ch layers due to the weak interlayer interaction. Indeed, as follows from the DOS calculations, the intercalation leads to a decrease in the Se 4p/Zr 4d energy gap width. A similar effect was observed for the InSe and GaSe layered materials.[101]

Conclusions

The experimental and theoretical study of the electronic structure of $ZrSe_2$ intercalated by copper was performed. The nonmonotonic filling of the tetra- and octahedral sites by the copper atoms

during the intercalation was found. The copper atoms partially move from the tetrahedral to octahedral sites in the concentration range of x = 0–0.2. The processing of the Cu $L_{2,3}$ XANES spectra for $Cu_{0.2}ZrSe_2$ demonstrates their additive character with contributions from the Cu atoms in the octahedral and tetrahedral sites. Cu 3p–3d ResPES indicates the increasing ionicity of the Zr–Cu chemical bond in the case of copper atoms occupying the octahedral sites. First principles calculations show that $ZrSe_2$ is a semiconductor with a direct energy gap. DOS calculations for $Cu_{0.125}ZrSe_2$ and $Cu_{0.25}ZrSe_2$ indicate that most pronounced changes at the Fermi level are observed for the Cu 3p states. In the case of the direct optical transitions the energy gap is estimated to be E_g = 0.8 eV and is almost independent of the copper concentration. As copper concentration increases, the semiconductor–metal transition occurs as a result of the Cu–Se hybridization and further saturation of this chemical bond. The impurity states involving Zr 4d electrons are formed as well leading to a gradual shift of the Fermi level at the conservation of a direct energy gap at the G point of the Brillouin zone.

At x > 0.2, the impurity band formed by the intercalated copper atoms overlaps with the $ZrSe_2$ conduction band, and the Fermi level moves to the conduction band, as it follows from the calculations of the electronic structure. Since copper forms impurity states in the Se 4p/Zr 4d energy gap, changing its concentration we can control the energy gap width.

The effect of the lattice defects on the electronic structure gives rise to another problem. One cannot avoid the formation of the different defects, but their concentration depends on the synthesis procedure. The prevalent defects are the extra Zr atoms (located in the van der Waals gap), which, in our opinion, make the main contribution to the Urbach defect absorption tail and provide the semiconducting behavior of the resistivity with an activation energy independent of the concentration of intercalated copper.

The observed competition between the occupation of the tetra- and octahedral sites by the copper atoms in Cu_xZrSe_2 is related to the competition between the formation of the impurity states in the Se 4p/Zr 4d energy gap on the one hand and the charge transfer from the copper atoms to the Zr 4d-derived conduction band on the other hand. This situation is possible due to a sufficiently wide Se 4p/Zr 4d energy gap, which is much wider than those in all previously studied intercalation compounds based on the transition metal dichalcogenides. We believe that a further increase in the band gap width (e.g., moving from $ZrSe_2$ to ZrS_2 or $HfSe_2$) will reinforce this trend by making the tetrahedral sites absolutely favorable in comparison with the octahedral ones.

Acknowledgements

The research was carried out within the state assignment of the Ministry of Science and Higher Education of the Russian Federation (theme ‘‘Spin’’ No. AAAA-A18-118020290104-2 theme and ‘‘Electron’’ No. AAAA-A18-118020190098-5). The magnetic susceptibility measurements and diffraction experiments were carried out at the Collective Equipment Center ‘‘Ural-M’’. We acknowledge Elettra Sincrotrone Trieste for providing access to its synchrotron radiation facilities. IP gratefully acknowledge financial support from EUROFEL.

References

1 J. A. Wilson and A. D. Yoffe, Adv. Phys., 1969, 18, 193–335. 2 J. A. Wilson, Phys. Status Solidi, 1978, 86, 11–36.

3 D. J. Eaglesham, R. L. Withers and D. M. Bird, J. Phys. C: Solid State Phys., 1986, 19, 359–367.

4 S. Balendhran, S. Walia, H. Nili, J. Z. Ou, S. Zhuiykov, R. B. Kaner, S. Sriram, M. Bhaskaran and K. Kalantar-zadeh, Adv. Funct. Mater., 2013, 23, 3952–3970. 5 Z. Kahraman, A. Kandemir, M. Yagmurcukardes and H. Sahin, J. Phys. Chem. C, 2019, 123(7), 4549–4557, DOI:

10.1021/acs.jpcc.8b11837.

6 X. Ding, F. Peng, J. Zhou, W. Gong, G. Slaven, K. P. Loh, C. T. Lim and D. T. Leong, Nat. Commun., 2019, 10, 41.

7 K. Rossnagel, J. Phys.: Condens. Matter, 2011, 23, 213001.

8 J. A. Wilson, F. J. Di Salvo and S. Mahajan, Adv. Phys., 1975, 24, 117–201.

9 A. H. Castro Neto, Phys. Rev. Lett., 2001, 86, 4382–4385.

10 T. Valla, A. V. Fedorov, P. D. Johnson, P.-A. Glans, C. McGuinness, K. E. Smith, E. Y. Andrei and H. Berger, Phys. Rev. Lett., 2004, 92, 086401.

11 W. Shi, J. Ye, Y. Zhang, R. Suzuki, M. Yoshida, J. Miyazaki, N. Inoue, Y. Saito and Y. Iwasa, Sci. Rep., 2015, 5, 12534. 12 D. C. Miller, S. D. Mahanti and P. M. Duxbury, Phys. Rev. B, 2018, 97, 045133.

13 M. S. Whittingham, Chem. Rev., 2004, 104, 4271–4302.

14 Y. Y. Lee, G. O. Park, Y. S. Choi, J. K. Shon, J. Yoon, K. H. Kim, W.-S. Yoon, H. Kim and J. M. Kim, RSC Adv., 2016, 6, 14253–14260.

15 M. Pumera, Z. Sofer and A. Ambrosi, J. Mater. Chem. A, 2014, 2, 8981–8987.

16 Y. Jing, Z. Zhou, C. R. Cabrera and Z. Chen, J. Phys. Chem. C, 2013, 117, 25409–25413.

17 X. Huang, Z. Zeng and H. Zhang, Chem. Soc. Rev., 2013, 42, 1934.

18 D. Chen, W. Chen, L. Ma, G. Ji, K. Chang and J. Y. Lee, Mater. Today, 2014, 17, 184–193.

19 S. Fan, X. Zou, H. Du, L. Gan, C. Xu, W. Lv, Y.-B. He, Q.-H. Yang, F. Kang and J. Li, J. Phys. Chem. C, 2017, 121, 13599–13605.

20 G. Barik and S. Pal, J. Phys. Chem. C, 2018, 122, 25837–25848.

21 K. Zhang, X. Fang, Y. Wang, Y. Wan, Q. Song, W. Zhai, Y. Li, G. Ran, Y. Ye and L. Dai, ACS Appl. Mater. Interfaces, 2017, 9, 5392–5398.

22 O. Lopez-Sanchez, D. Lembke, M. Kayci, A. Radenovic and A. Kis, Nat. Nanotechnol., 2013, 8, 497–501.

23 K. Roy, M. Padmanabhan, S. Goswami, T. P. Sai, G. Ramalingam, S. Raghavan and A. Ghosh, Nat. Nanotechnol., 2013, 8, 826–830.

24 V. Podzorov, M. E. Gershenson, C. Kloc, R. Zeis and E. Bucher, Appl. Phys. Lett., 2004, 84, 3301–3303.

25 B. Radisavljevic, A. Radenovic, J. Brivio, V. Giacometti and A. Kis, Nat. Nanotechnol., 2011, 6, 147–150.

26 J. Yu, C.-H. Lee, D. Bouilly, M. Han, P. Kim, M. L. Steigerwald, X. Roy and C. Nuckolls, Nano Lett., 2016, 16, 3385–3389. 27 A. N. Titov, E. G. Shkvarina, L. N. Zelenina, T. P. Chusova and M. R. Sharafutdinov, Phys. Solid State, 2016, 58, 735–741.

28 A. S. Shkvarin, Y. M. Y. M. Yarmoshenko, A. I. Merentsov, Y. M. Y. M. Zhukov, A. A. A. N. A. A. Titov, E. G. Shkvarina and A. A. A. N. A. A. Titov, Phys. Chem. Chem. Phys., 2017, 19, 4500–4506.

29 E. G. Shkvarina, S. G. Titova, A. N. Titov and A. S. Shkvarin, J. Alloys Compd., 2017, 717, 286–293. 30 Y. Arnaud, M. Chevreton, A. Ahouandjinou, M. Danot and J. Rouxel, J. Solid State Chem., 1976, 18, 9–15. 31 G. Calvarin, J. R. Gavarri, M. A. Buhannic, P. Colombet and M. Danot, Rev. Phys. Appl., 1987, 22, 1131–1138.

32 M. Danot and R. Brec, Acta Crystallogr., Sect. B: Struct. Crystallogr. Cryst. Chem., 1975, 31, 1647–1652. 33 M. Danot, J. Bichon and J. Rouxel, Bull. Soc. Chim. Fr., 1972, 3063.

34 E. Morosan, H. W. Zandbergen, B. S. Dennis, J. W. G. Bos, Y. Onose, T. Klimczuk, A. P. Ramirez, N. P. Ong and R. J. Cava, Nat. Phys., 2006, 2, 544–550. 35 R. B. Somoano and A. Rembaum, Phys. Rev. Lett., 1971, 27, 402–404.

36 R. B. Somoano and J. A. Woollam, in Intercalated layered materials, ed. F. Levy, Reidel, Dordrecht, Holland, 1979, p. 307.

37 N. Ahmad, P. C. Klipstein, S. D. Obertelli, E. A. Marseglia and R. H. Friend, J. Phys. C: Solid State Phys., 1987, 20, 4105–4114.

38 Y. Tazuke and T. Takeyama, J. Phys. Soc. Jpn, 1997, 66, 827–830.

39 D. R. Huntley, M. J. Sienko and K. Hiebl, J. Solid State Chem., 1984, 52, 233–243.

40 V. G. Pleschov, N. V. Baranov, A. N. Titov, K. Inoue, M. I. Bartashevich and T. Goto, J. Alloys Compd., 2001, 320, 13–17.

41 Y. S. Hor and R. J. Cava, Mater. Res. Bull., 2009, 44, 1375–1378.

42 S. He´bert, W. Kobayashi, H. Muguerra, Y. Bre´ard, N. Raghavendra, F. Gascoin, E. Guilmeau and A. Maignan, Phys. Status Solidi, 2013, 210, 69–81.

43 H. I. Starnberg, H. E. Brauer, L. J. Holleboom and H. P. Hughes, Phys. Rev. Lett., 1993, 70, 3111–3114. 44 W. Jaegermann, Surface Studies of Layered Materials in Relation to Energy Converting Interfaces, 1992, pp. 195–295.

45 J. Khan, C. M. Nolen, D. Teweldebrhan, D. Wickramaratne, R. K. Lake and A. A. Balandin, Appl. Phys. Lett., 2012, 100, 043109.

46 M. M. Thackeray, J. O. Thomas and M. S. Whittingham, MRS Bull., 2000, 25, 39–46.

47 F. J. Di Salvo, D. E. Moncton and J. V. Waszczak, Phys. Rev. B: Solid State, 1976, 14, 4321–4328.

48 C. Monney, E. F. Schwier, M. G. Garnier, N. Mariotti,

C. Didiot, H. Cercellier, J. Marcus, H. Berger, A. N. Titov,

H. Beck and P. Aebi, New J. Phys., 2010, 12, 125019. 49 J. van Wezel, P. Nahai-Williamson and S. S. Saxena, Phys. Rev. B: Condens. Matter Mater. Phys., 2010, 81, 165109.

50 A. F. Kusmartseva, B. Sipos, H. Berger, L. Forro´ and E. Tutisˇ, Phys. Rev. Lett., 2009, 103, 236401. 51 H. E. Brauer, H. I. Starnberg, L. J. Holleboom and

H. P. Hughes, J. Phys.: Condens. Matter, 1995, 7, 7741–7760. 52 H. Isoma¨ki and J. von Boehm, Phys. Scr., 1981, 24, 465–467.

53 G. Tenorio, L. Bucio and R. Escudero, J. Supercond. Novel Magn., 2017, 30, 2381–2386.

54 Z. Muhammad, K. Mu, H. Lv, C. Wu, Z. ur Rehman, M. Habib, Z. Sun, X. Wu and L. Song, Nano Res., 2018, 11, 4914–4922.

55 A. S. Shkvarin, A. I. Merentsov, Y. M. Yarmoshenko, M. S. Postnikov, E. G. Shkvarina, A. A. Titov, I. Pis, S. Nappini, F. Bondinoand A. N.Titov, J.Phys.Chem.C, 2019,123,410–416.

56 E. G. Shkvarina, A. A. Titov, A. A. Doroschek, A. S. Shkvarin,

D. V. Starichenko, J. R. Plaisier, L. Gigli and A. N. Titov,

J. Chem. Phys., 2017, 147, 044712.

57 A. A. Titov, E. G. Shkvarina, A. I. Merentsov, A. A. Doroshek,

A. S. Shkvarin, Y. M. Zhukov, A. G. Rybkin, S. V. Pryanichnikov, S. A. Uporov and A. N. Titov, J. Alloys Compd., 2018, 750, 42–54. 58 G. D. Cody, J. Non-Cryst. Solids, 1992, 141, 3–15.

59 A. S. Shkvarin, A. I. Merentsov, E. G. Shkvarina, Y. M. Yarmoshenko, I. Pı´ˇs, S. Nappini and A. N. Titov, J. Chem. Phys., 2018, 148, 124707.

60 H. P. B. Rimmington, A. A. Balchin and B. K. Tanner, J. Cryst. Growth, 1972, 15, 51–56.

61 A. C. Larson and R. B. Von Dreele, Doc. LAUR, 1994, 86–748. 62 E. Prince, in International tables for crystallography, ed. A. J. C. Wilson, Kluwer, 2004, vol. 100.

63 M. Zangrando, M. Finazzi, G. Paolucci, G. Comelli, B. Diviacco, R. P. Walker, D. Cocco and F. Parmigiani, Rev. Sci. Instrum., 2001, 72, 1313.

64 J. P. Perdew, K. Burke and M. Ernzerhof, Phys. Rev. Lett., 1996, 77, 3865–3868.

65 ELK – open access code http//elk.sourceforge.net/.

66 R. Gaillac, P. Pullumbi and F.-X. Coudert, J. Phys.: Condens. Matter, 2016, 28, 275201.

67 T. Hibma, in Intercalation Chemistry, ed. M. S. Wittingham and A. J. Jacobsen, London, Acad. Press, 1982, pp. 285–313. 68 A. N. Titov, Phys. Solid State, 2009, 51, 714–720.

69 A. N. Titov, A. V. Kuranov, V. G. Pleschev, Y. M. Yarmoshenko,

M. V. Yablonskikh, A. V. Postnikov, S. Plogmann, M. Neumann, A. V. Ezhov and E. Z. Kurmaev, Phys. Rev. B: Condens. Matter Mater. Phys., 2001, 63, 035106.

70 A. V. Postnikov, M. Neumann, S. Plogmann, Y. M. Yarmoshenko, A. N. Titov and A. V. Kuranov, Comput. Mater. Sci., 2000, 17, 450–454.

71 A. S. Shkvarin, Y. M. Yarmoshenko, N. A. Skorikov, A. A. Titov and A. N. Titov, J. Exp. Theor. Phys., 2012, 114, 324–328.

72 A. S. Shkvarin, Y. M. Yarmoshenko, M. V. Yablonskikh, A. I. Merentsov, E. G. Shkvarina, A. A. Titov, Y. M. Zhukov and A. N. Titov, J. Chem. Phys., 2016, 144, 074702.

73 R. Z. Bachrach, Synchrotron Radiation Research: Advances in Surface and Interface Science Techniques, Springer Science & Business Media, 2012, vol. 1.

74 A. Kay, E. Arenholz, S. Mun, F. J. G. de Abajo, C. S. Fadley, R. Denecke, Z. Hussain and M. A. Van Hove, Science, 1998, 281, 679–683.

75 J.-E. Rubensson, J. Lu¨ning, S. Eisebitt and W. Eberhardt, Appl. Phys. A: Mater. Sci. Process., 1997, 65, 91–96.

76 N. Mårtensson, M. Weinelt, O. Karis, M. Magnuson, N. Wassdahl, A. Nilsson, J. Sto¨hr and M. Samant, Appl. Phys. A: Mater. Sci. Process., 1997, 65, 159–167.

77 S. Hu¨fner, S.-H. Yang, B. S. Mun, C. S. Fadley, J. Scha¨fer, E. Rotenberg and S. D. Kevan, Phys. Rev. B: Condens. Matter Mater. Phys., 2000, 61, 12582–12585.

78 J.J.YehandI.Lindau,At.DataNucl.DataTables,1985,32,1–155. 79 Y. M. Yarmoshenko, A. S. Shkvarin, M. V. Yablonskikh, A. I. Merentsov and A. N. Titov, J. Appl. Phys., 2013, 114, 133704.

80 V. V. Sobolev and V. V. Nemoshkalenko, Methods of computational physics in solid theory: Electronic structure of rare-metal dichalcogenides, Naukova Dumka, 1990.

81 S. G. Patel, M. K. Agarwal, N. M. Batra and D. Lakshminarayana, Bull. Mater. Sci., 1998, 21, 213–217.

82 H. Luo, J. W. Krizan, E. M. Seibel, W. Xie, G. S. Sahasrabudhe,

S. L. Bergman, B. F. Phelan, J. Tao, Z. Wang, J. Zhang and

R. J. Cava, Chem. Mater., 2015, 27, 6810–6817.

83 S. Ahmad, R. D'Souza and S. Mukherjee, Mater. Res.

Express, 2018, 6, 036308.

84 J. I. Pankove, Optical processes in semiconductors, Courier Corporation, 1975.

85 D. Errandonea, A. Mun˜oz, P. Rodrı´guez-Herna´ndez, J. E. Proctor, F. Sapin˜a and M. Bettinelli, Inorg. Chem., 2015, 54, 7524–7535.

86 M. Moustafa, T. Zandt, C. Janowitz and R. Manzke, Phys.

Rev. B: Condens. Matter Mater. Phys., 2009, 80, 035206.

87 A. H. Reshak and S. Auluck, Phys. B, 2004, 353, 230–237. 88 R. B. Murray and A. D. Yoffe, J. Phys. C: Solid State Phys., 1972, 5, 3038–3046.

89 D. W. Bullett, J. Phys. C: Solid State Phys., 1978, 11, 4501–4514.

90 J. von Boehm and H. M. Isomaki, J. Phys. C: Solid State Phys., 1982, 15, L733–L737.

91 T. Hibma, M. S. Whittingham and A. J. Jacobson, Intercalation Chemistry, Academic Press, London, 1982. 92 W. Salomons and G. A. Wiegers, Recl. Trav. Chim. Pays-Bas, 1968, 87(12), 1339–1344, DOI: 10.1002/recl.19680871202. 93 D. van der Putten and R. Zanoni, Phys. Lett. A, 1995, 208, 351–355.

94 S. Kashida, W. Shimosaka, M. Mori and D. Yoshimura, J. Phys. Chem. Solids, 2003, 64, 2357–2363.

95 T. V. Kuznetsova, V. I. Grebennikov, H. Zhao, C. Derks,

C. Taubitz, M. Neumann, C. Persson, M. V. Kuznetsov, I. V. Bodnar, R. W. Martin and M. V. Yakushev, Appl. Phys. Lett., 2012, 101, 111607.

96 V. V. Bozhko, A. V. Novosad, O. V. Parasyuk, O. Y. Khyzhun,

N. Vainorius, A. Nekrosˇius, V. Vertelis and V. Kaˇzukauskas,

J. Phys. Chem. Solids, 2015, 82, 42–49.

97 D. K. G. De Boer, C. F. Van Bruggen, G. W. Bus,

R. Coehoorn, C. Haas, G. A. Sawatzky, H. W. Myron, D. Norman and H. Padmore, Phys. Rev. B: Condens. Matter Mater. Phys., 1984, 29(12), 6797–6809, DOI: 10.1103/ PhysRevB.29.6797.

98 R. Claessen, R. O. Anderson, G.-H. Gweon, J. W. Allen,

W. P. Ellis, C. Janowitz, C. G. Olson, Z. X. Shen, V. Eyert and M. Skibowski, Phys. Rev. B: Condens. Matter Mater. Phys., 1996, 54(4), 2453–2465, DOI: 10.1103/PhysRevB.54.2453.

99 J. C. E. Rasch, T. Stemmler, B. Mu¨ller, L. Dudy and R. Manzke, Phys. Rev. Lett., 2008, 101(23), 237602, DOI: 10.1103/ PhysRevLett.101.237602.

100 H. Wang, Z. Qiu, W. Xia, C. Ming, Y. Han, L. Cao, J. Lu, P. Zhang, S. Zhang, H. Xu and Y. Y. Sun, J. Phys. Chem. Lett., 2019, 10(22), 6996–7001, DOI: 10.1021/acs.jpclett. 9b02710.

101 D. Errandonea, A. Segura, F. J. Manjo´n, A. Chevy, E. Machado, G. Tobias, P. Ordejo´n and E. Canadell, Phys. Rev. B: Condens. Matter Mater. Phys., 2005, 71, 125206.

Figures and Tables

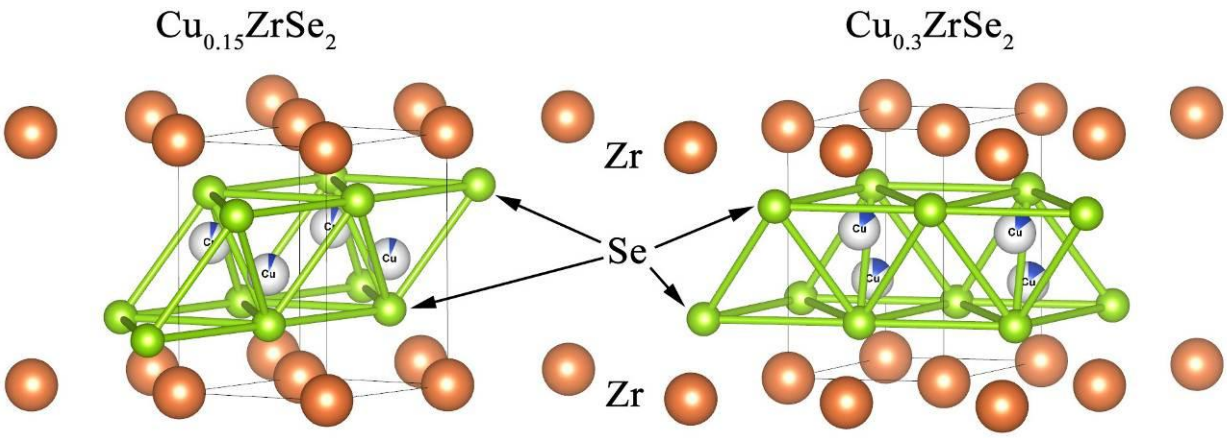

Figure 1. A fragment of the crystal structure of CuxZrSe2 (x = 0.15 and 0.3). The copper atoms are shown in tetrahedral sites. For x = 0.15 Cu atoms are located closer to the vertex of the tetrahedron (ZCu = 0.458), for x = 0.3 – closer to the base of the tetrahedron (ZCu = 0.629).

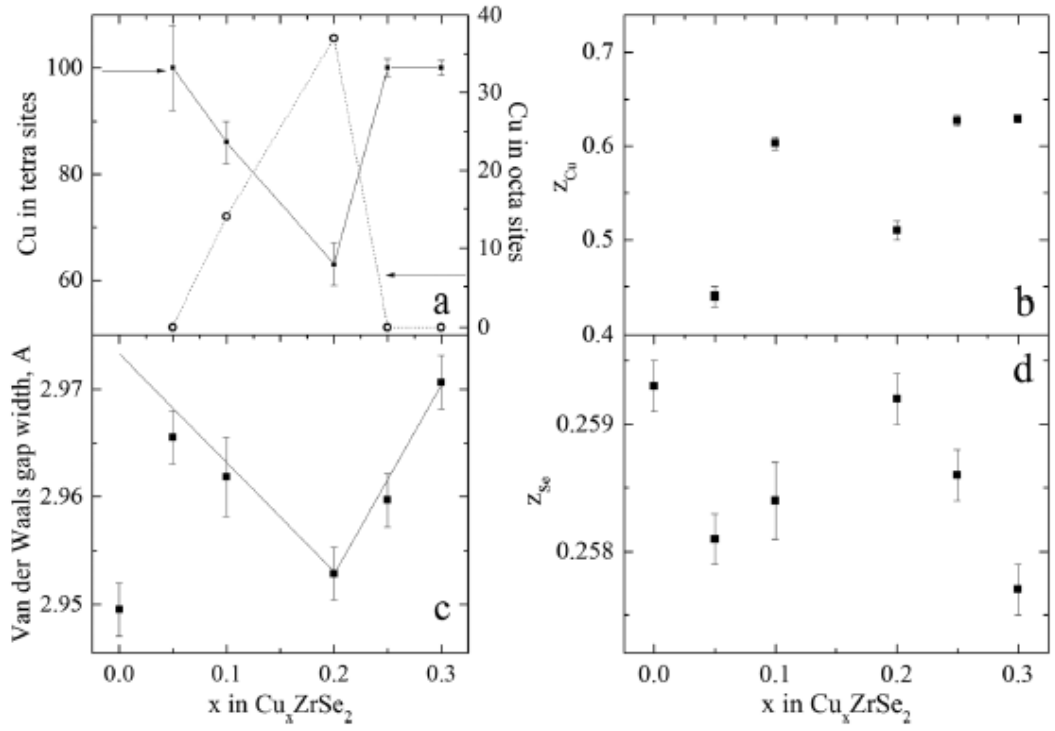

Figure 2. Concentration dependence of the CuxZrSe2 lattice parameters ($0 \le x \le 0.3$): (a) fraction of the Cu atoms in the tetrahedral (left Y axis) and octahedral (right Y axis) sites; (b) z coordinate of the Cu atom in the tetrahedral site; (c) van der Waals gap width; (d) z coordinate of the Se atom.

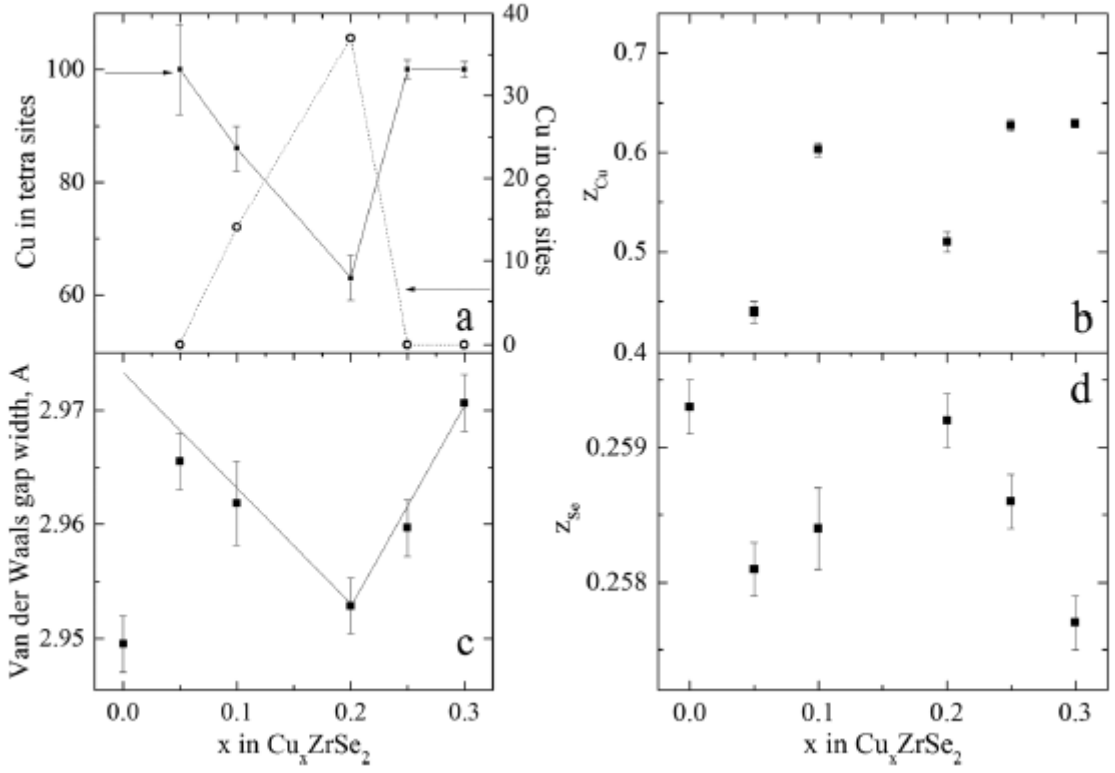

Figure 3. Upper panel: Cu L2.3 XANES for CuxZrSe2. Lower panel: Difference Cu L2.3 XANES for Cu0.2ZrSe2 and Cu L2.3 XANES for Cu0.33TiSe2.

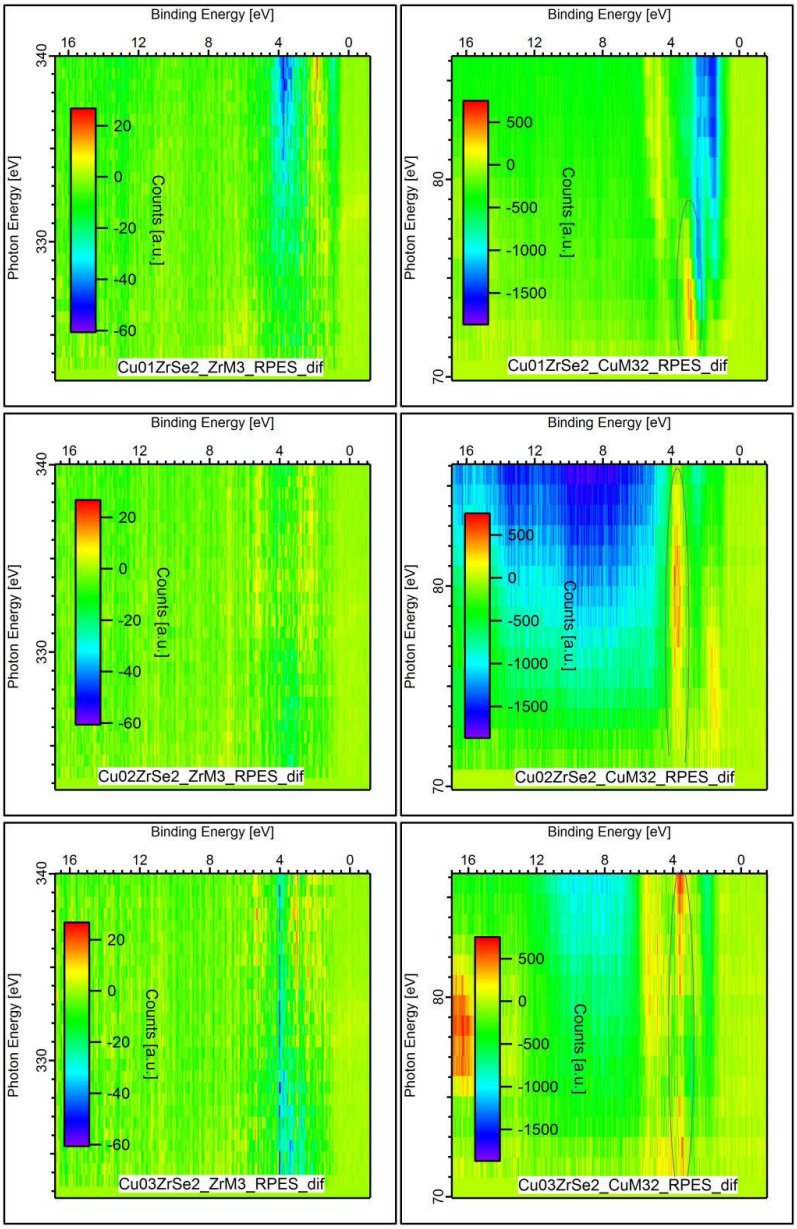

Figure 4. The Zr 3p3/2–4d ResPES (left panels) and Cu 3p–3d ResPES (right panels) difference spectra for Cu0.1ZrSe2, Cu0.2ZrSe2 and Cu0.3ZrSe2 (the processing method is described in ref. 79) in the form of image plot.

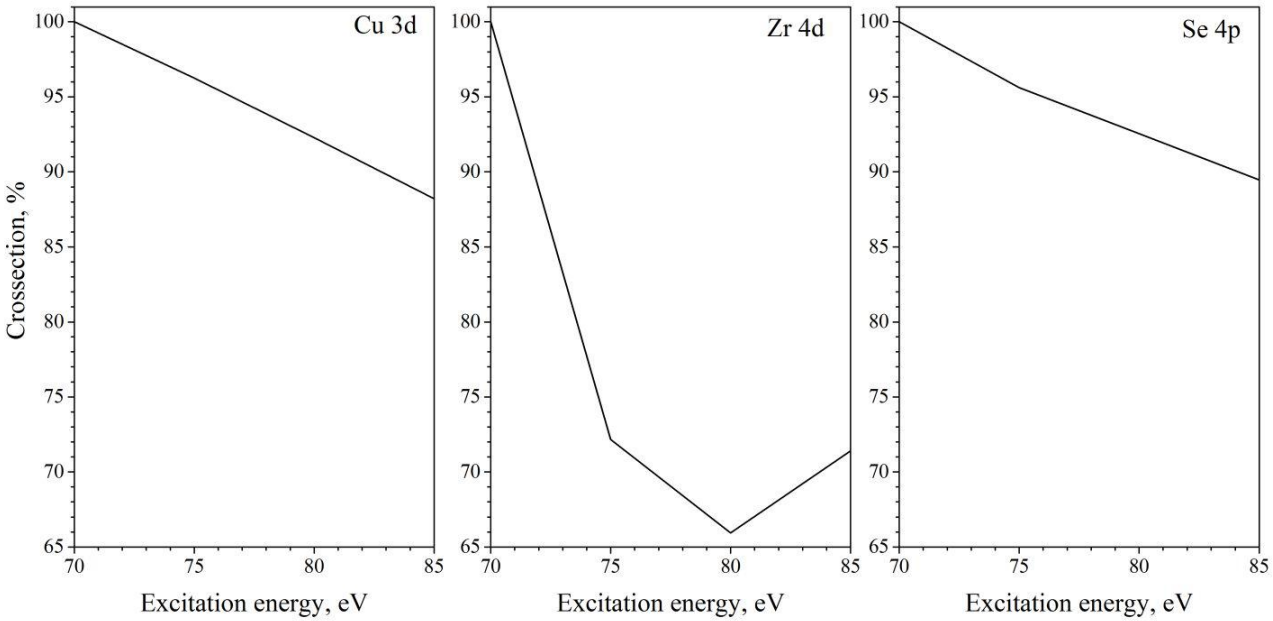

Figure 5. Relative (to the value for Eexc = 70 eV) photoionization cross-sections for Cu 3d, Zr 4d and Se 4p according to ref. 78 depending on the excitation energy.

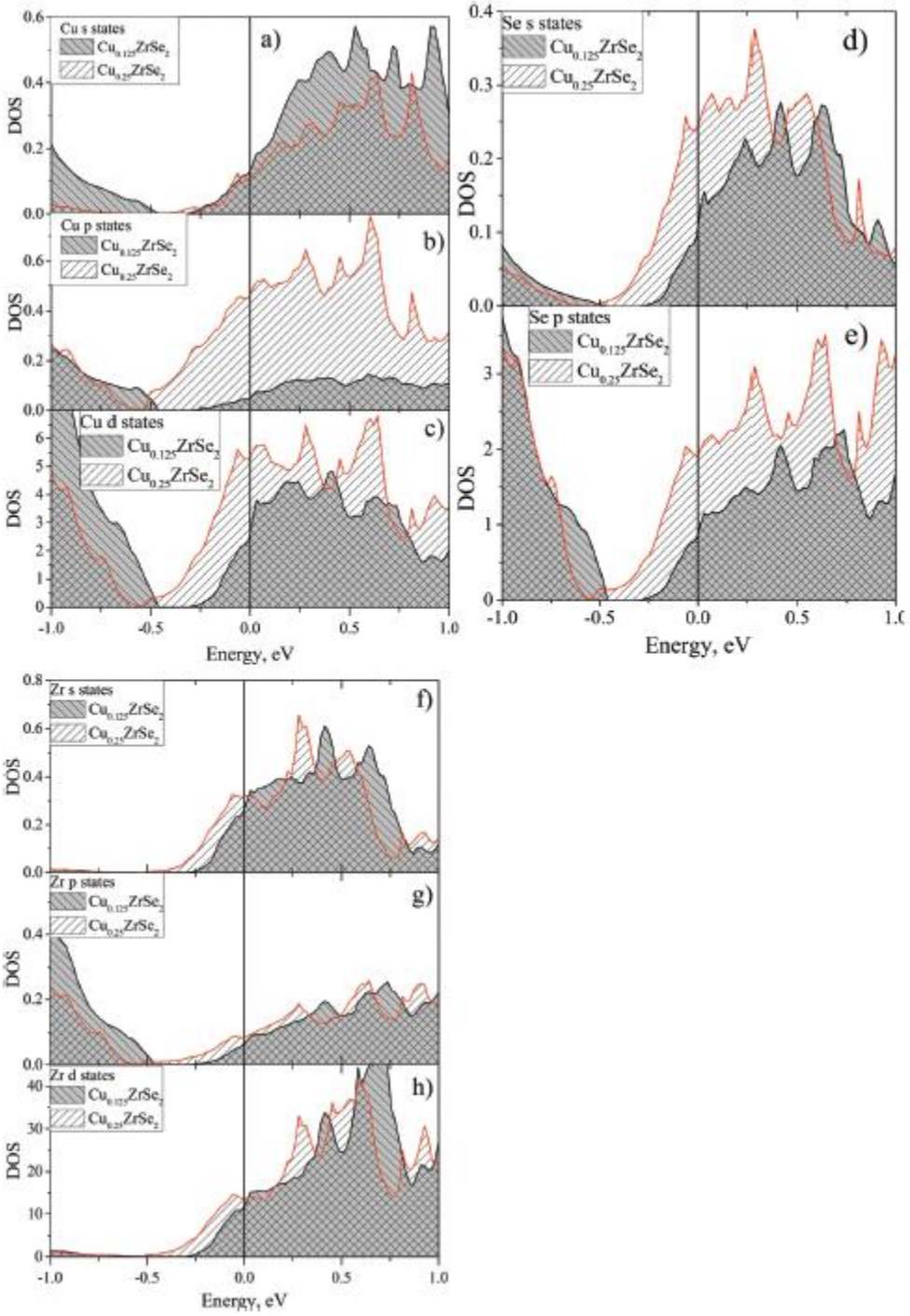

Figure 6. Cu s (a), Cu p (b), Cu d (c), Se s (d), Se p (e), Zr s (f), Zr p (g), and Zr d (h) partial DOS for Cu0.125ZrSe2 and Cu0.25ZrSe2.

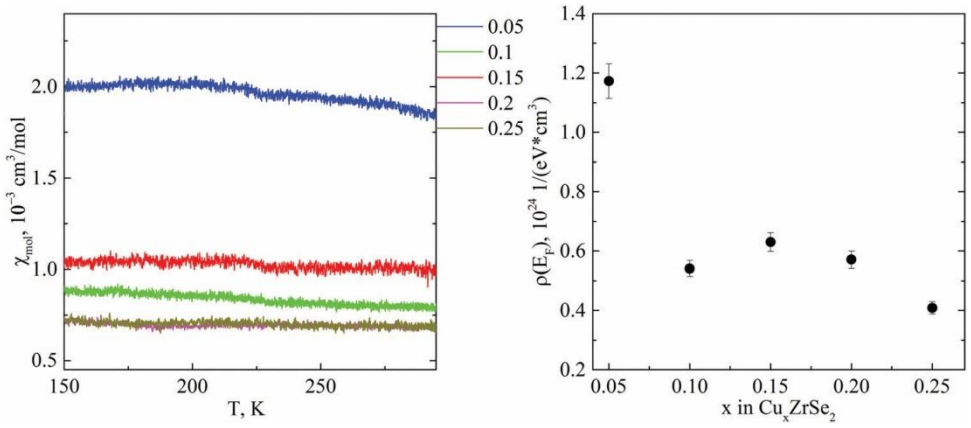

Figure 7. Left panel: Temperature dependence of the molar magnetic susceptibility for CuxZrSe2. Right panel: Copper concentration dependence of the calculated DOS at the Fermi level.

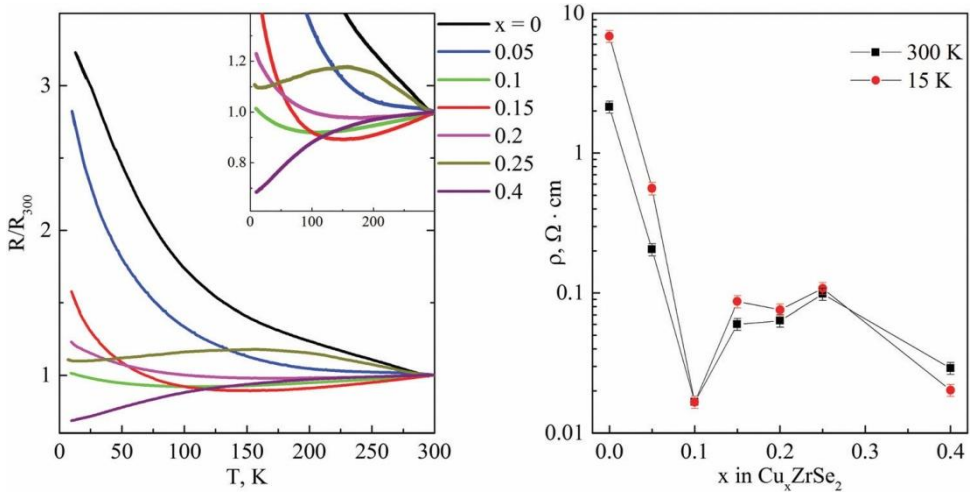

Figure 8. Left panel: Temperature dependence of the resistance R normalized to the room temperature value R300; in the inset – the image enlarged in the R/R300 axis (the units are the same as for the main axes). Right panel: Copper concentration dependence of the conductivity for CuxZrSe2.

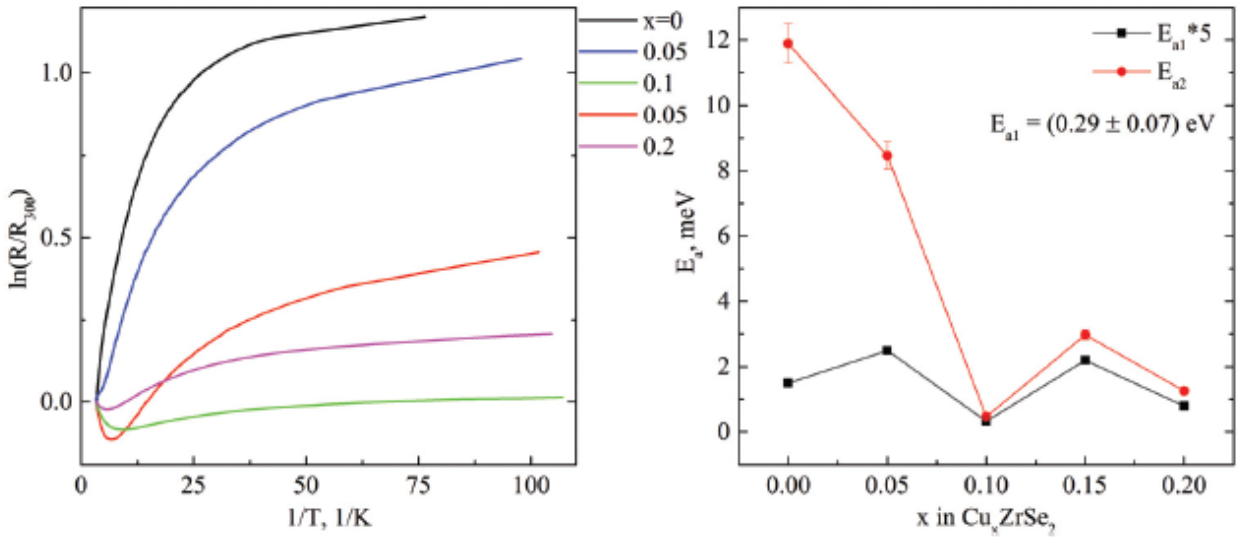

Figure 9. Left panel: The temperature dependence of the resistivity plotted in $\ln(R/R_{300})$ vs. 1/T coordinates. Right panel: Activation energies E_{a1} (squares) (multiplied by 5) and E_{a2} (circles) as a function of the copper concentration. Since E_{a1} does not depend on the copper concentration and its value is substantially lower than that of E_{a2}, the averaged value of E_{a1} is given as well. The errors for all the E_{a1} points and for E_{a2} points at $x \geq 0.1$ do not exceed the point size.

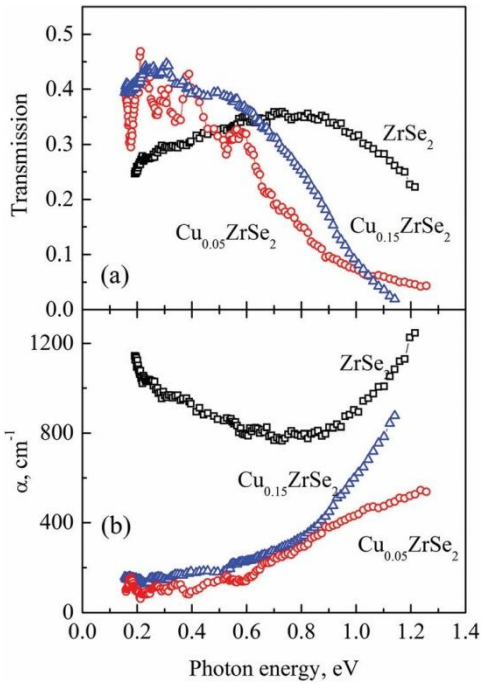

Figure 10. The transmission (a) and absorption coefficient (b) for ZrSe2, Cu0.05ZrSe2 and Cu0.15ZrSe2.

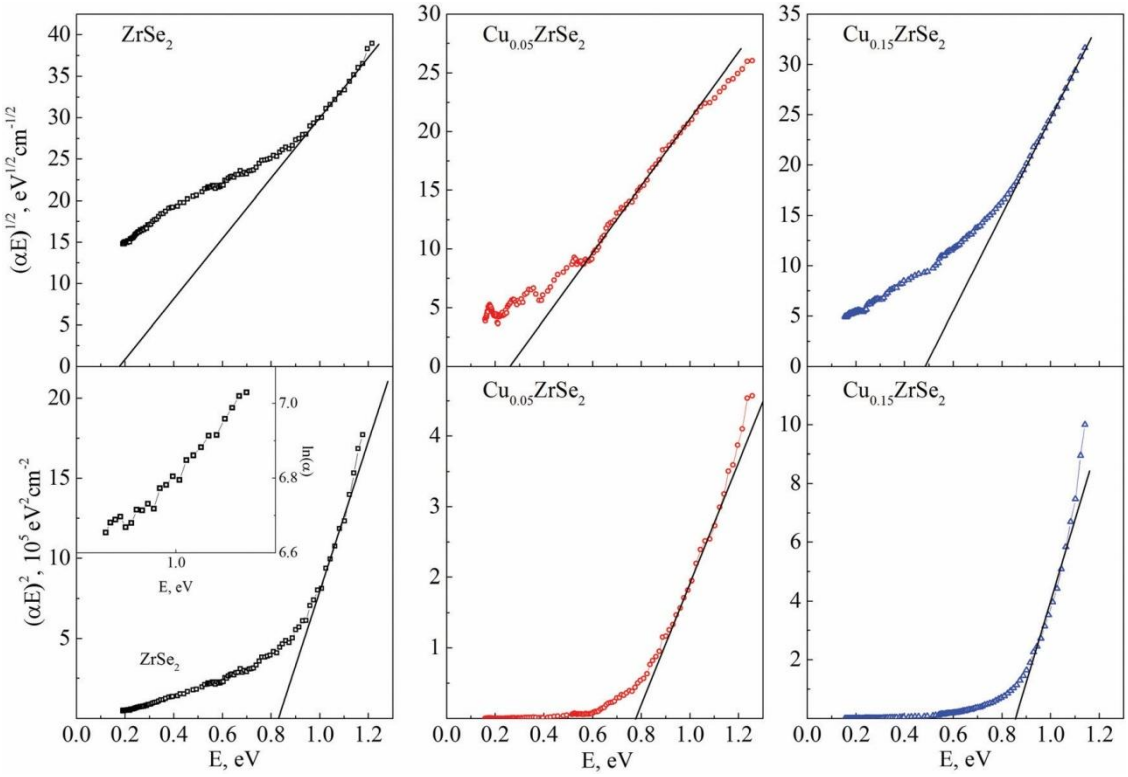

Figure 11. Optical absorption for the crystals $ZrSe_2$, $Cu_{0.05}ZrSe_2$ and $Cu_{0.15}ZrSe_2$ plotted as $(\alpha\hbar\omega)^{1/2}$ vs. $\hbar\omega$ for indirect transitions (upper panel) and $(\alpha\hbar\omega)^2$ vs. $\hbar\omega$ for direct transitions (lower panel). The inset shows $\ln(\alpha)$ vs. the photon energy for $ZrSe_2$.

	a, Å	c, Å	Z_{Se}	$Z_{tetra_{Cu}}$	Fraction Cu^{tetra}	Fraction Cu^{octa}	R_F^2, %	χ^2
$ZrSe_2$	3.770(1)	6.127(1)	0.2593(2)	—	—	—	5.59	4.146
$Cu_{0.05}ZrSe_2$	3.771(1)	6.131(1)	0.2579(2)	0.68(3)	0.024(2)	0	3.24	2.841
$Cu_{0.1}ZrSe_2$	3.771(1)	6.130(1)	0.2584(3)	0.603(7)	0.043(2)	0.014(5)	3.45	2.732
$Cu_{0.2}ZrSe_2$	3.771(1)	6.131(1)	0.2592(2)	0.51(1)	0.063(4)	0.074(8)	4.36	2.352
$Cu_{0.25}ZrSe_2$	3.771(1)	6.130(1)	0.2586(2)	0.627(6)	0.125(2)	0	4.93	2.899
$Cu_{0.3}ZrSe_2$	3.771(1)	6.130(1)	0.2577(2)	0.629(4)	0.150(2)	0	3.78	2.624

Table 1. The results of the crystal structure refinement for the Cu_xZrSe_2 ($0 \le x \le 0.3$) compounds. a, c – lattice parameters; Z_{Se} – z-coordinate of the selenium atom; Z^{tetra}_{Cu} – z-coordinate of the copper atom which occupy the tetrahedral site; fraction Cu^{tetra} – fraction (in mol%) of the copper atoms which occupy the tetrahedral sites; fraction Cu^{octa} – fraction (in mol%) of the copper atoms which occupy the octahedral sites; $R_F^2 = (\Sigma_{hkl}(F_{O,hkl}^2 - F_{C,hkl}^2))/\Sigma_{hkl}F_{O,hkl}^2$; $\chi^2 = (R_{wp}/R_{exp})^2$

Electronic Supplementary Material (ESI) for Journal of Materials Chemistry C.

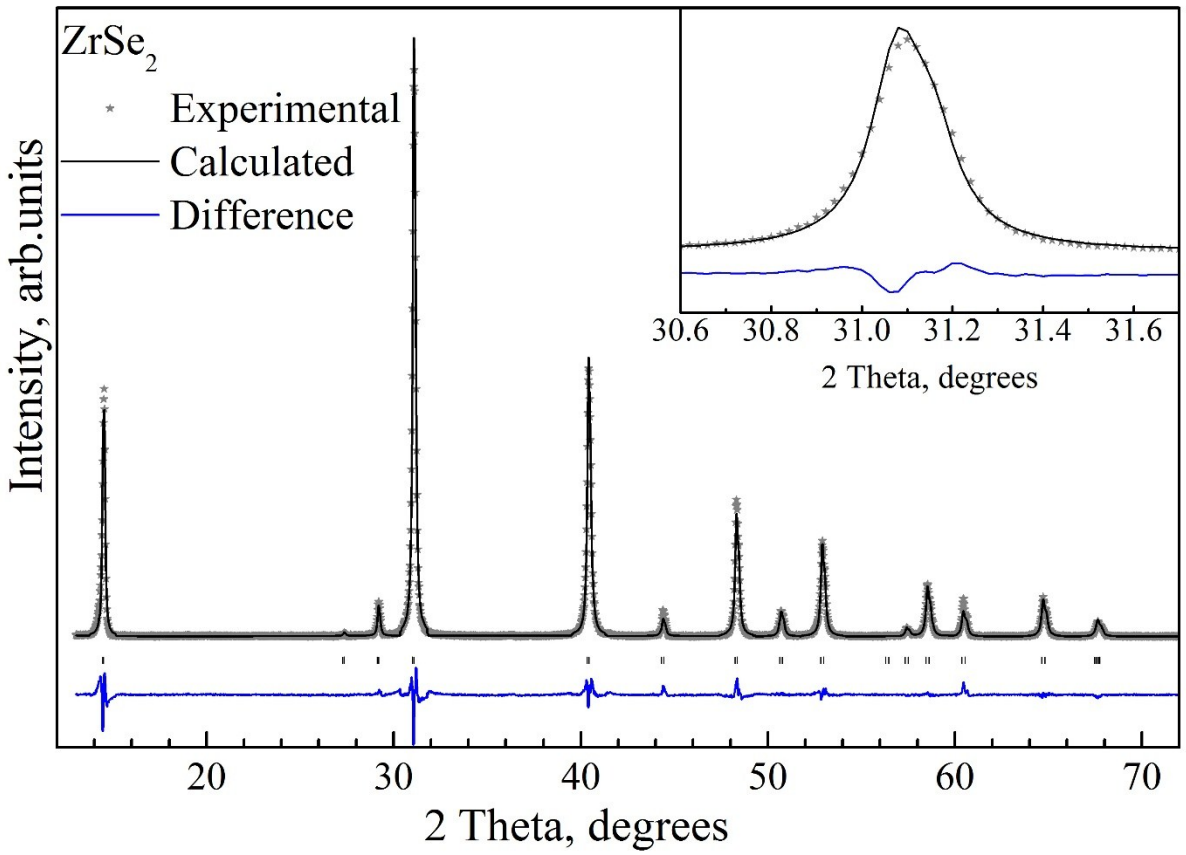

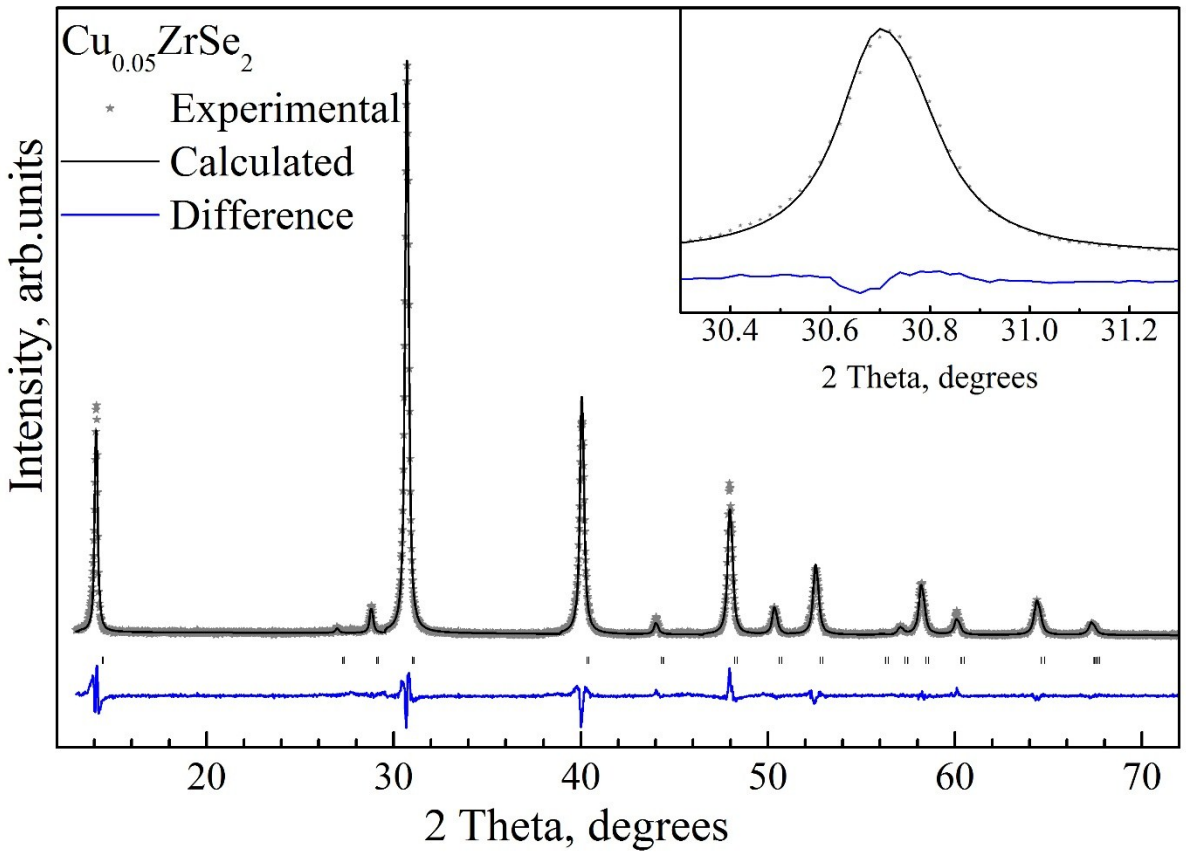

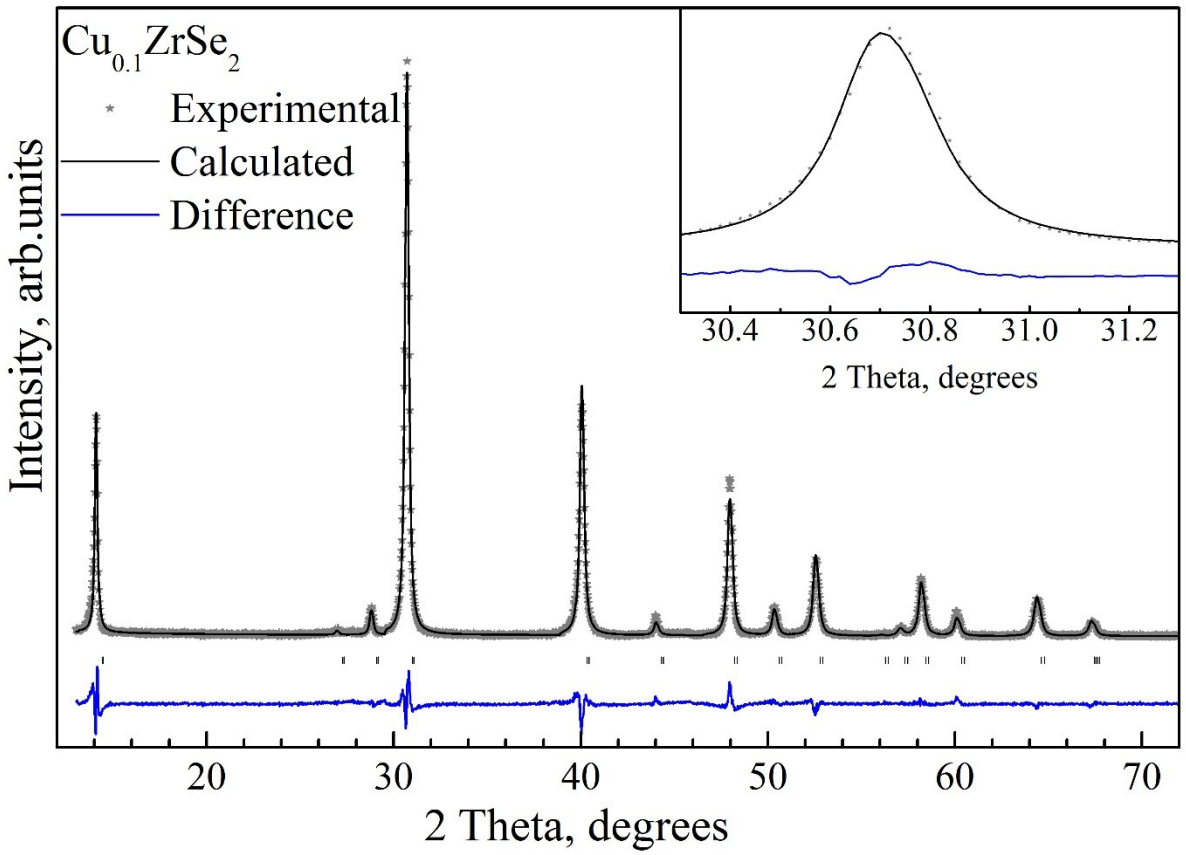
Cu0.1ZrSe2
Experimental
Calculated
Difference
Intensity, arb.units
2 Theta, degrees
30.4
30.6
30.8
31.0
31.2
2 Theta, degrees
20
30
40
50
60
70
2 Theta, degrees

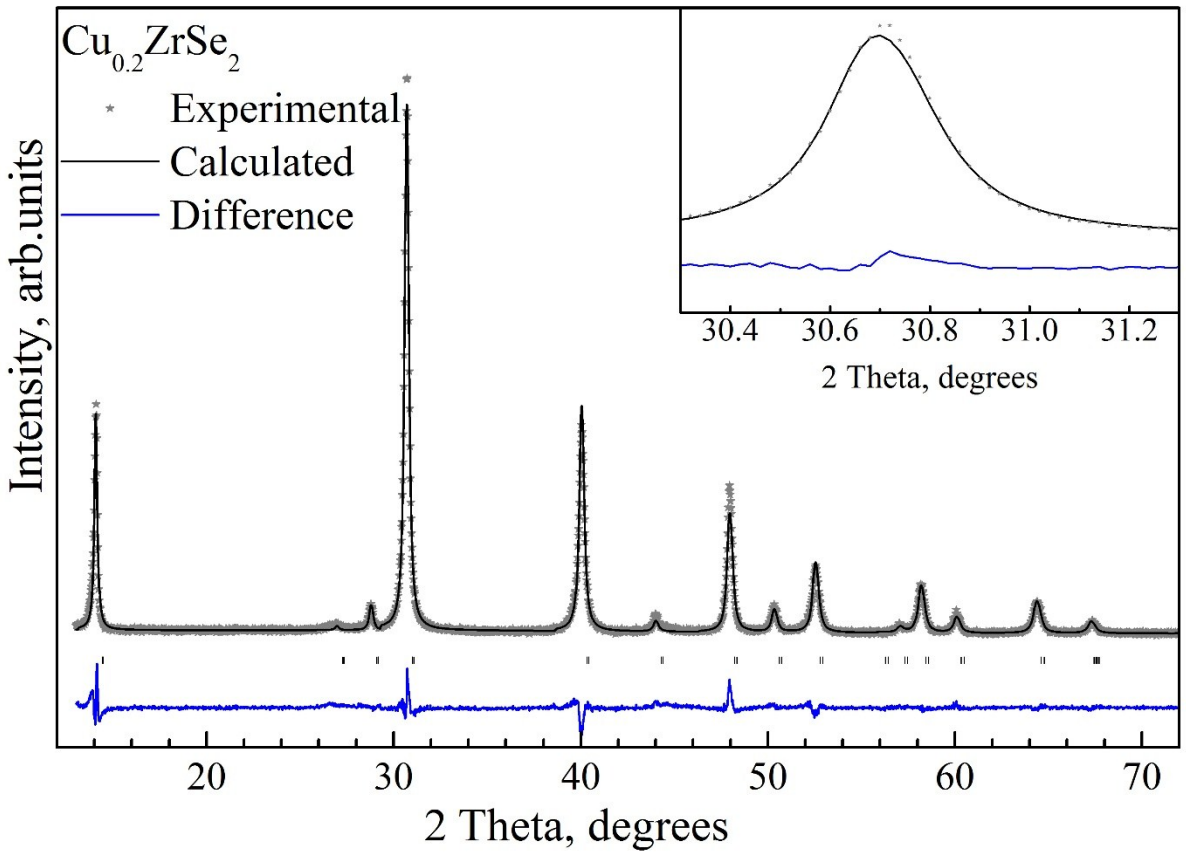
Cu0.2ZrSe2
Experimental
Calculated
Difference
Intensity, arb.units
2 Theta, degrees
30.4
30.6
30.8
31.0
31.2
2 Theta, degrees
20
30
40
50
60
70
2 Theta, degrees

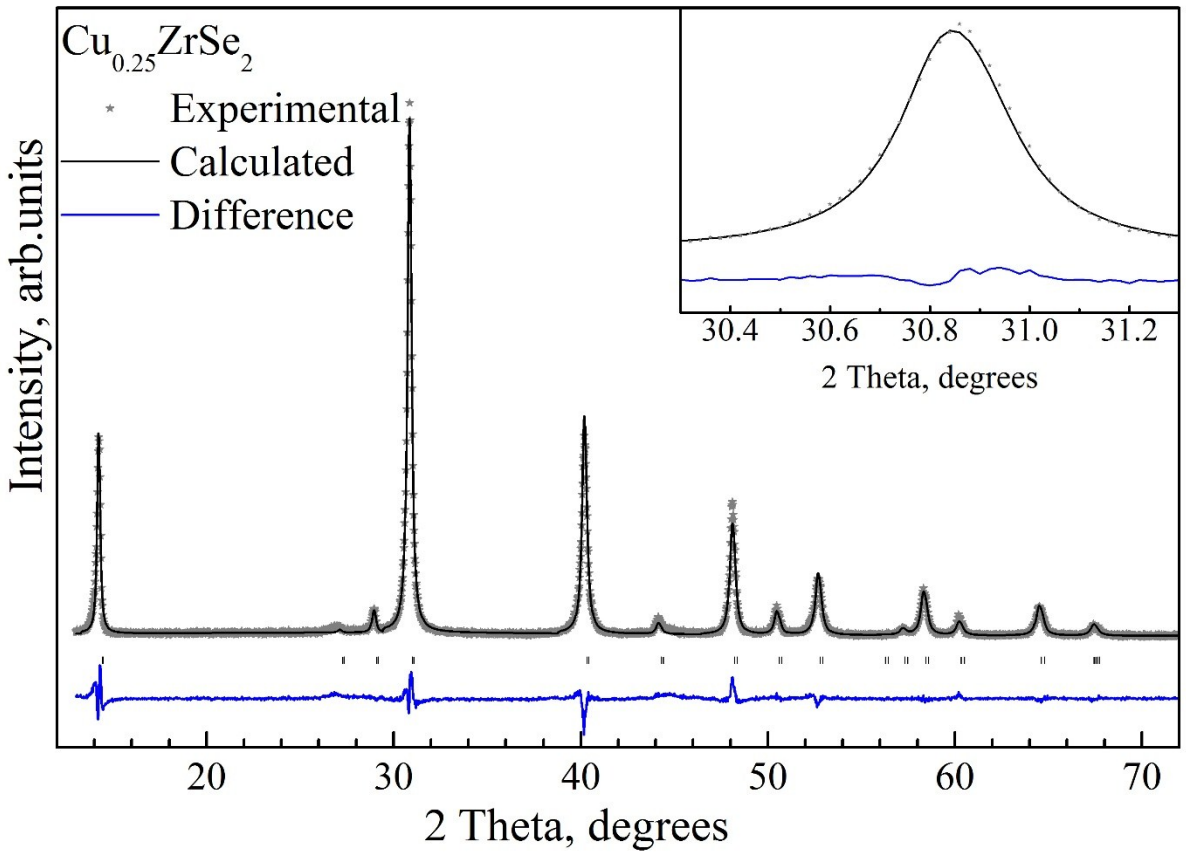
Cu0.25ZrSe2
Experimental
Calculated
Difference
Intensity, arb.units
2 Theta, degrees
30.4
30.6
30.8
31.0
31.2
2 Theta, degrees
20
30
40
50
60
70
2 Theta, degrees

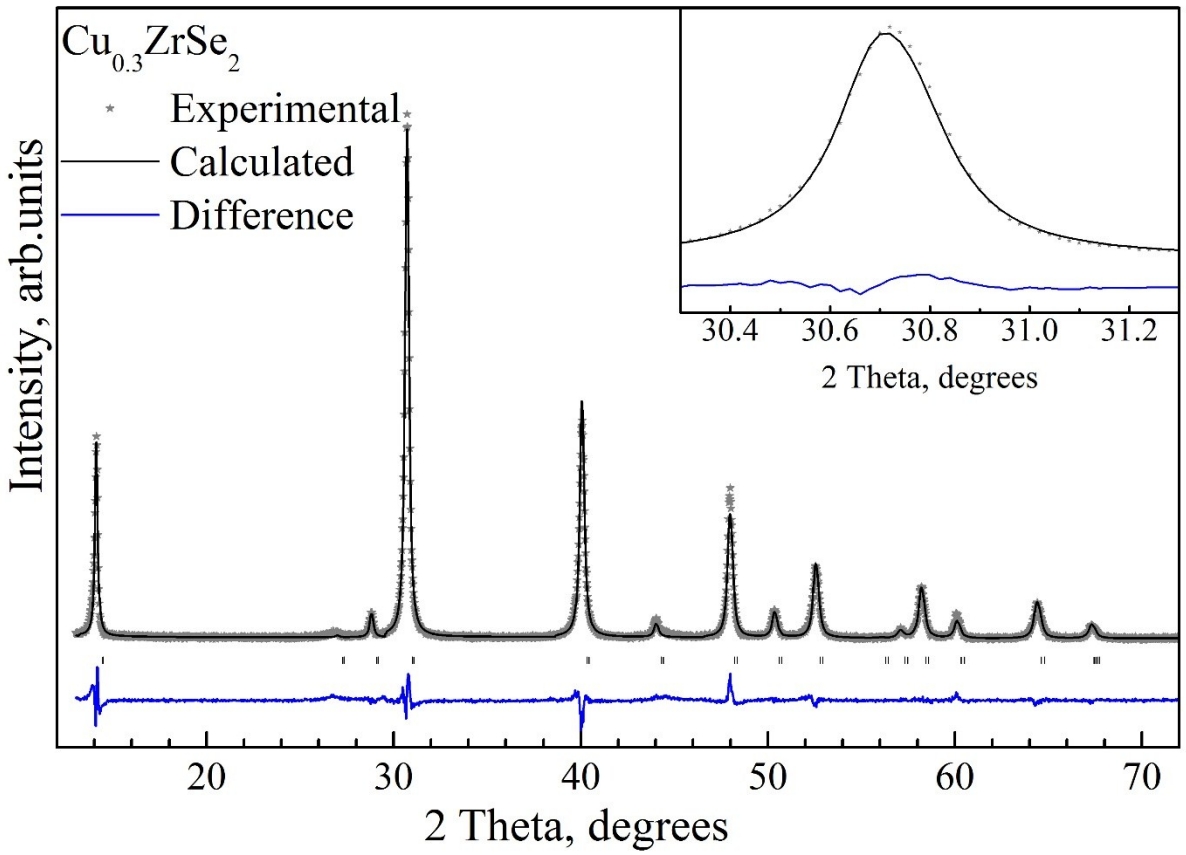
Cu0.3ZrSe2
Experimental
Calculated
Difference
Intensity, arb.units
2 Theta, degrees
30.4
30.6
30.8
31.0
31.2
2 Theta, degrees
20
30
40
50
60
70
2 Theta, degrees